Abstract

CAVANAUGH, CURTIS C. An Adaptive Electronic Interface for Gas Sensors (Under the direction of H. Troy Nagle).

This thesis focuses on the development of an adaptive electronic interface for gas sensors that are used in the NC State electronic nose. We present an adaptive electronic interface that allows for the accurate mapping of the sensor's voltage output to sensor resistance profiles. The adaptive interface uses a linearized Wheatstone bridge in a constant current configuration. The balancing of the bridge and the adjustment of the subsequent gain stage is performed using programmable variable resistors. The programmable resistors are controlled by a LabVIEW® program. The same control program also determines and records all the resistor values in the interface circuit. The resistance of each sensor is accurately computed by LabVIEW® using the interface-circuit resistor values and the voltage output of the circuit. Compensating for sensor drift can be done in LabVIEW® by adjusting the programmable resistor values so that a zero-voltage output is produced during the reference cycle. By doing this zero adjustment between each "sniff" of an odorant, the baseline drift can be minimized.

A single channel of the adaptive electronic interface has been designed and tested. The interface can be calibrated so that it is 99% accurate when performing sensor resistance measurements.

A new conducting polymer sensor chamber has also been designed and tested. The new radial flow sensor chamber minimizes the dead volume in the chamber and also delivers the odorant to each sensor at the same time. Two operating modes were compared: continuous-flow and sniff-and-hold. Both modes gave good classification performance while testing four different coffee samples. Experimental testing indicates that sensor response is highly correlated with the sample flow rate. Future work to more fully characterize this correlation is recommended.

AN ADAPTIVE ELECTRONIC INTERFACE FOR GAS SENSORS

by

CURTIS CAVANAUGH

A thesis submitted to the Graduate Faculty of

North Carolina State University

in partial fulfillment of the

requirements for the Degree of

Master of Science

ELECTRICAL ENGINEERING

Raleigh

2002

APPROVED BY:

Edward Grant, Ph.D.

Mark White, Ph.D.

H. Troy Nagle, Ph.D., M.D.

Chair of Advisory Committee

Dedication

This thesis is dedicated to my three-month old son Evan Winfield Cavanaugh. I learned from his birth how insignificant everything else really is. Now that I am finished, I can dedicate more of my time to him.

Biography

CURTIS CAVANAUGH was born in West Palm Beach, FL. After graduation from Southwide Academy in 1989, he entered military service in the United States Marine Corps. During his military service he worked as an electronics technician at the Marine Corps Logistics Base, Albany, GA and at Camp Lejeune, NC. Upon completion of military service, he worked for several years as an electronics technician at Electrical South Limited Partnership in Greensboro, NC while taking college courses at the University of North Carolina at Greensboro. In the spring of 1998, he entered North Carolina State University. He received the B.S. degree in Electrical Engineering from North Carolina State University in 2000. He entered the Graduate Program in Electrical Engineering at North Carolina State University in 2000. During the following year he worked in the Biomedical Instrumentation Laboratory.

Acknowledgements

This project would not have been successful without the efforts of several people. First and foremost, I would like to thank my wonderful wife Kimberly for her support and encouragement.

I would to thank my advisor, Dr. Troy Nagle, whose continuous guidance and support helped me throughout this project. I am also grateful to the other members of my advisory committee, Dr. Eddie Grant and Dr. Mark White. I also want to thank Dr. Susan Schiffman of Duke University for her advice and for letting me perform experiments in the Duke Taste and Smell Laboratory.

Dr. Dick Guarnieri has been very supportive and helpful during this project as well as Sridhar Kashyap, Bruce Linnell, and Rehka Balasubramanium.

Larry DuFour of the Precision Instrument Machine Shop in the College of Engineering has greatly contributed to this project as well and I am deeply indebted to him.

Table of Contents

List of Tables

List of Figures

Chapter 1. Background

1.1 The Human Olfactory System

Understanding how a biological olfactory system works is the first step in designing an electronic nose because an electronic nose must mimic a biological olfactory system. The human olfactory system is described here.

1.1.1 Olfactory Mucous Membrane

The anatomy of the human olfactory system is illustrated in Figure 1.1. The process of olfaction in humans begins when volatile organic compounds are inhaled through the nostrils and are transported to the olfactory mucous membrane. Low concentrations of odorants in the inspired air must pass through the mucous membrane covering the nasal epithelium before making contact with the olfactory chemoreceptors. The mucus layer (see Figure 1.2) contains an abundance of small, water-soluble proteins that act as carrier proteins and also bind odorants.

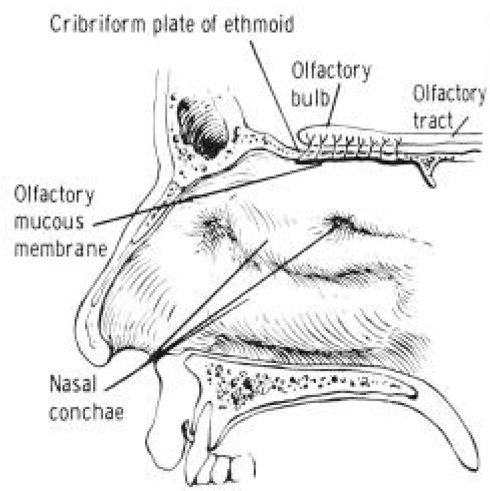

Figure 1.1 Human Olfactory System [1]

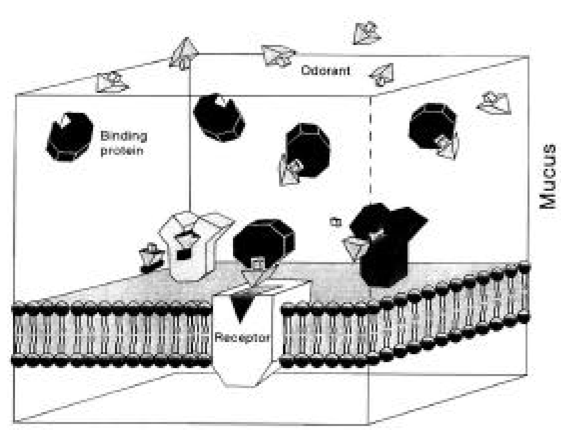

Figure 1.2 Odorant Binding Proteins [2]

There are 10 – 20 million receptor cells interspersed among the supporting cells of the mucous membrane. The receptor cells have extensions called dendrites that carry electrical signals into the cell body. Projecting from the dendrites into the surface of the mucus layer are microtubular hair-like structures called cilia (see Figure 1.3). The odorant binding proteins in the mucus layer shuttle the odorant towards the cilia. As the odorant interacts with the cilia, information about the odorant is transmitted from the receptor cell out through its axon to the olfactory bulb.

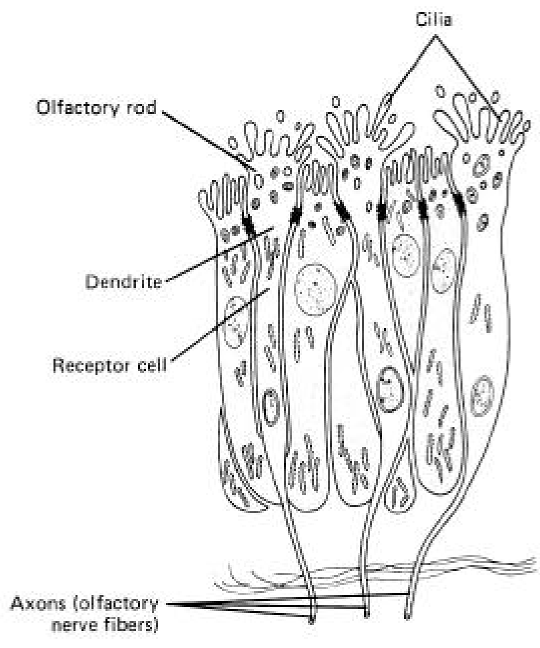

Figure 1.3 Receptor Cells [1]

1.1.2 Olfactory Bulbs [1]

In the olfactory bulbs, the axons of the receptors terminate and form the olfactory glomeruli. An average of 26,000 receptor cell axons converge on each glomerulus. Impulses concerned with olfactory reflexes are passed from the glomeruli to the rest of the limbic system and the hypothalamus.

1.1.3 Physiology of Olfaction

The olfactory receptors only respond to substances that are dissolved in contact with the olfactory epithelium. Several theories exist as to the reaction that occurs when odoriferous molecules react with a receptor. One theory holds that odoriferous molecules inactivate enzyme systems in the epithelium, altering its chemical reactions [1]. Another theory holds that the molecules alter the surface of the receptor cells, thus changing their electrical state [1]. A third theory holds that the molecules simply alter the sodium-ion permeability of the receptor membrane [1].

1.1.4 Odorants

The human nose can tell the difference between about 10,000 different odors [3]. The structures of the chemicals that give odor sensation are very diverse. There does not appear to be any structural requirement for a molecule to be an odorant. It must, however, be volatile enough to reach the olfactory epithelium. Generally, odor producing molecules are those containing between 3 and 20 carbon atoms. For the most part, molecules that have a molecular weight greater than 300 are odorless [3].

Two things that determine odor description are the size and shape of the odorant molecule along with the distribution of polar groups [2]. However, the exact structural requirements for specifying an odor are not known and the presence of polar groups in certain odorants can be correlated with a distinctive odor type. With small molecules, polar groups play an important part in the interaction with the olfactory receptors. The influence of polar groups on large molecules is much less.

1.2 Electronic Nose Basics

According to Gardner [4],

> *“an electronic nose is an instrument, which combines an array of electronic chemical sensors with partial specificity and an appropriate pattern-recognition system, capable of recognizing simple or complex odours”.*

The partial specificity of the sensors in the array combined with the pattern recognition module provide the electronic nose with a wider range of odor detection capabilities than with individual sensors alone.

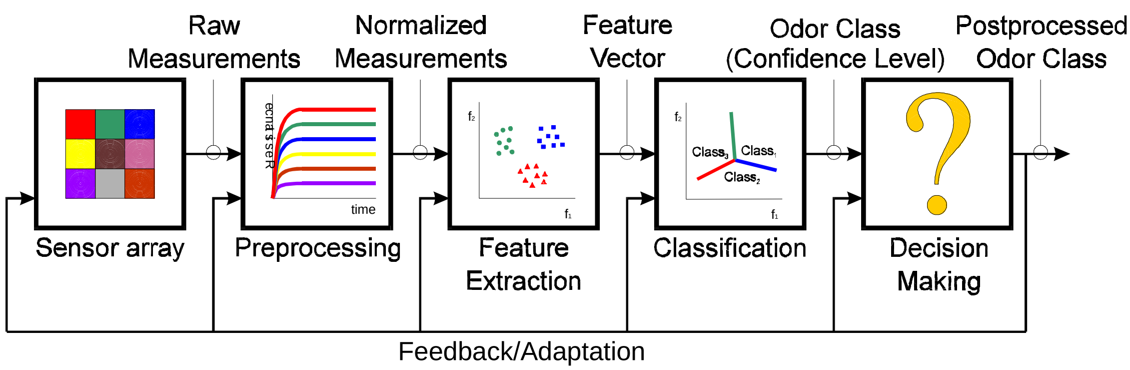

Figure 1.4 Electronic Nose Block Diagram [7]

A block diagram showing the components that constitute an electronic nose is shown in Figure 1.4. The diagram has five separate blocks: sensor array, preprocessing, feature extraction, classification, and decision making. The sensor array consists of a number of sensors with broad specificity. Preprocessing can be used to compensate for sensor drift, normalize the sensor data, and compress the sensor response. Feature extraction reduces the dimensionality of the measurement space and extracts information for classification purposes. The classification module assigns a class label to an unknown sample based on the information contained in the entire data set or on previously recorded data. The final decision making block uses application specific information to modify the classifier assignment and to enhance the accuracy of the system.

1.2.1 Gas Sensors

Many types of gas sensors are in use in Electronic Nose research. The most common types of sensors used in Electronic Noses are conductivity sensors (Metal Oxide Semiconductor and Conducting Polymer types); Metal Oxide Semiconductor Field Effect Transistors (MOSFET), optical sensors, and piezoelectric sensors. The sensors used in the North Carolina State University (NC State) E-Nose are conductivity sensors and the background discussion here is limited to this type of sensor only.

- **Metal Oxide Semiconductors**

Metal oxide semiconductor (MOS) sensors have been used extensively in electronic nose instruments and are readily available commercially [6]. Typical offerings include oxides of tin, zinc, titanium, tungsten, and iridium, doped with a noble metal catalyst such as platinum

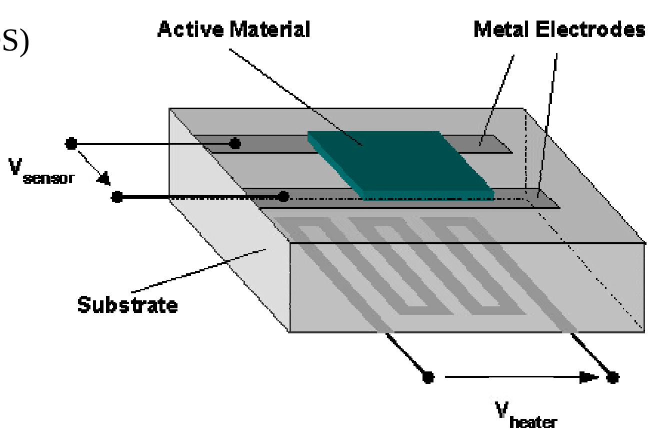

Figure 1.5 MOS sensor

or palladium [5]. The metal oxide semiconductor is deposited between two electrodes and over a heating element (see Figure 1.5) that operates at temperatures from 200°C - 400°C. Because of the high operating temperature, power consumption is a particular concern in applications that require a portable, hand-held instrument.

The mechanism most responsible for gas reactions with MOS in air at elevated temperatures is the change in the concentration of the adsorbed oxygen at the sensor surface [6]. As oxygen ions form at the surface of the sensor, the charge carrier density decreases. As the number of charge carriers decrease, the conductivity of the sensor decreases and the change in the semiconductor resistance can be measured during this reaction. The oxide, the doping material, and the operating temperature can control sensor selectivity and sensitivity. The sensitivity of MOS sensors ranges from 5 to 500 parts per million (ppm). A drawback of MOS sensors is that they respond to humidity. Small changes in humidity from sample to sample can overwhelm even smaller changes that occur in odorant concentration.

- **Conducting Polymers**

Simple conducting polymer sensors are made up of two electrodes with a conductive polymer coating between them. As shown in Figure 1.6, the active material is a conducting

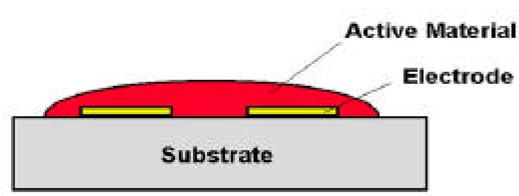

Figure 1.6 Conducting polymer sensor

polymer from such families that include polypyrroles, thiophenes, indoles, or furans. Changes in the conductivity of these materials occur as they are exposed to the various types of chemicals that interact with the polymer backbone [5]. The interaction of gas with the sensor surface affects the transfer of electrons along the polymer chain. It is this reaction that changes the sensor conductivity.

Fabrication of these sensors involves forming two electrodes separated by a gap of 10 to 20 micrometers. The conducting polymer is then deposited between the two electrodes [5]. The response time of the sensor is inversely proportional to the polymer's thickness. Because conducting polymer sensors operate at ambient temperatures, they do not need heaters.

1.2.2 Data Pre-processing

Preprocessing can be used to compensate for sensor drift, normalize the sensor data, and compress the sensor response [7].

- **Drift Removal**

Gas sensors tend to drift over time. Mechanisms that cause sensor drift include odorant retention in the active material, humidity changes, and temperature variations. Generally, compensating for drift is done using software after the data has been collected. A common compensation technique is that of subtracting the initial sensor value from the rest of the data for that measurement. An example of sensor drift is shown in Figure 1.7.

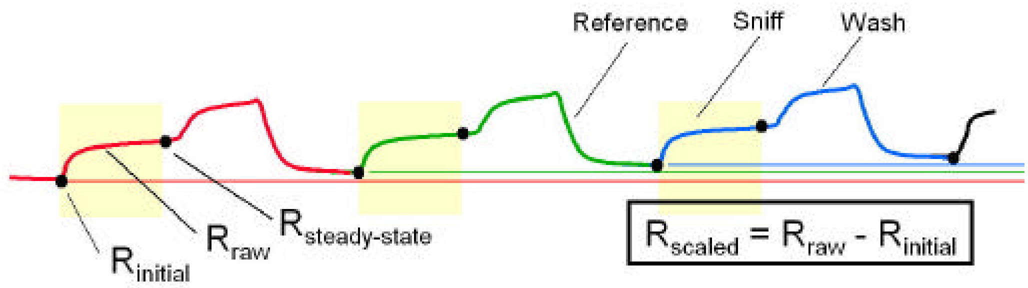

Figure 1.7 Sensor drift

- **Normalization**

Normalizing the sensor data can be achieved by dividing the sensor data by its maximum value. Doing this ensures that the maximum value of the data is one. This allows for comparison of data without regard to the amplitude of the sensor response. A visual representation of normalization is shown in Figure 1.8.

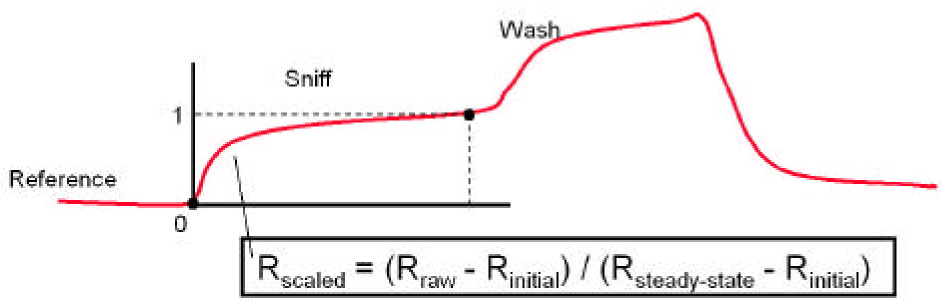

Figure 1.8 Sensor data normalization

- **Compression**

Data preprocessing compression operations are used to reduce the number of measurements per example. For an array with 15 sensors, a sampling frequency of 1.0 Hz for 60 seconds of transient response, the number of measurements totals 900. The common procedure used in many commercial instruments is to record only the steady state or final value of each sensor (15 measurements in the example above) and disregard the transient [8]. However, the transient conveys useful information. Windowed time slicing has been shown to be an effective compression method. The transient response is multiplied by N_W smooth, bell-shaped windowing functions like the ones in Figure 1.9, and integrated with respect to time. The number of windowing functions is arbitrary, but $N_W=4$ was chosen for consistency with Kermani [9].

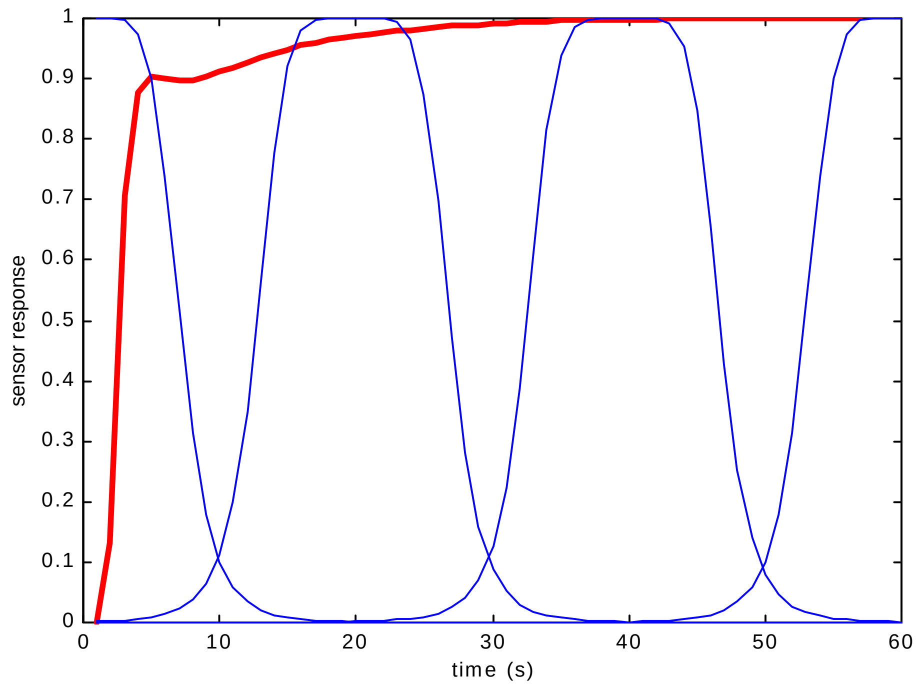

Figure 1.9 Bell-shaped kernels for windowed time slicing

1.2.3 Feature Extraction

Feature extraction is the process of transforming the measurement space into a feature space of lower dimensionality while simultaneously extracting relevant information for pattern recognition. Two feature extraction transforms that are widely regarded in the pattern recognition literature are Principal Components Analysis (PCA) and Linear Discriminant Analysis (LDA).

- **Principal Components Analysis (PCA)**

  Principal Components Analysis (also known as the Karhunen-Loève transform in communication theory) is the oldest technique in multivariate analysis. First introduced by Pearson in 1901 [10], it experienced several modifications until it was generalized by Loève in 1963 [11]. The objective of PCA is to perform dimensionality reduction of the measurement space yet still preserve as much randomness in the data as possible. The main limitation of PCA is that it does not consider class separability; it does not take into account the class label of the samples [8].

- **Linear Discriminant Analysis (LDA)**

Linear Discriminant Analysis was presented by Fisher in 1936 [12] and is probably the oldest technique still widely used in pattern recognition. The goal of LDA is to find a lower-dimensional representation of a random vector x that maximizes class separability.

1.2.4 Pattern Recognition

The classification module assigns a class label to an unknown sample based on the entire data set or on previously recorded data.

- **Artificial Neural Networks**

Neurons are the fundamental building blocks of the human nervous system. Each neuron consists of a single cell with the ability to receive signals from many other cells. The point at which one signal passes from one neuron to another is called a synapse. In 1949, Hebb [13] proposed that the behavior of these synapses is modified during learning. It is this idea of modifiable interconnected networks which forms the basis of artificial neural computing [14]. In an artificial neural network, the neuron is replaced by a simple processing element. The output from a processing element is connected to the input of another element through what are known as connection weights. The value of these weights can be modified, thus giving the system the ability to learn. A network consists of a large number of processing elements connected together through their associated connection weights.

- **Decision Tree Induction**

Decision trees are used regularly in data mining [15]. They are rooted with simple classifiers placed at each internal node and a classification at each leaf. Decision trees are generally learned by means of a top down growth procedure, starting at the root node and greedily choosing a split of the data to maximize some cost function. Typically, the simple classifier at an internal node compares one of the input attributes against a threshold. A widely used algorithm of this kind is C4.5 [15].

- **Genetic Algorithms**

Genetic algorithms are optimization methods inspired by and modeled after natural evolution. Genetic algorithms are relatively simple, yet are not limited by restrictive assumptions about the search space like continuity or smoothness [16]. They have the ability to capture the global view of a problem and not be overwhelmed by local details. Basically, genetic algorithms are based on Darwin's theory of evolution. The genetic algorithm starts with a set of solutions, called the population. Solutions are extracted from the population and are further used to form a new population, with the intent that the new population will be a better fit. This process is repeated until some condition (for example, a specific number of populations or improvement of the best solution) is satisfied. Kermani [9] used this method to improve the performance of E-nose data processing algorithms.

1.3 References

[1] Ganong, W.F. Review of Medical Physiology. 9th ed. Los Altos, CA: Lang Medical Publications, 1979.

[2] Breer, H. "Sense of smell: Signal recognition and transduction in olfactory receptor neurons." Handbook of Biosensors and Electronic Noses. Ed. E. Kress-Rogers. Boca Raton, FL: CRC Press LLC, 1997.

[3] Persaud, K.C. and Travers, P.J. "Arrays of broad specificity films for sensing volatile chemicals." Handbook of Biosensors and Electronic Noses. Ed. E. Kress-Rogers. Boca Raton, FL: CRC Press LLC, 1997.

[4] Gardner, J.W. and Bartlett, P.N. "A brief history of electronic noses." Sensors and Actuators B, Chemical, 18-19, pp. 211-220. 1994.

[5] Nagle, H.T., Schiffman, S.S. and Gutierrez-Osuna, R. "The How and Why of Electronic Noses." IEEE Spectrum. September 1998.

[6] Hoffheins, B. "Solid state, resistive gas sensors." Handbook of Chemical and Biological Sensors. Eds. R.F. Taylor and J.S. Schultz. Philadelphia: Institute of Physics Publishing, 1996.

[7] Gutierrez Osuna, R., and Nagle, H.T. "A method for evaluating Data Preprocessing Techniques for odor Classification with an array of gas sensors." IEEE transactions on System, Man & Cybernetics, Part B, Vol 29. October 1999.

[8] Gutierrez Osuna, R. "Signal processing and pattern recognition for an electronic nose." Ph.D. Dissertation, Electrical and Computer Engineering Department, North Carolina State University, 1998.

[9] Kermani, B. G., "On using neural networks and genetic algorithms to optimize the performance of an electronic nose." Ph.D. Dissertation, Electrical and Computer Engineering Department, North Carolina State University, 1996.

[10] Pearson, K. "On lines and planes of closest fit to systems of points in space." Philosophical Magazine 2, 559-572. 1901.

[11] Loève, M. Probability Theory, 3rd ed. New York: Van Nostrand, 1963.

[12] Fisher, R. A. "The use of multiple measurements in taxonomic problems." Annals of Eugenics. Vol. 7(II), 179-188. Cambridge: Francis Galton Laboratory for National Eugenics, University of London, 1925 - 1954.

[13] Hebb, D.O. The organization of behavior: a neuro-psychological theory. New York: Wiley, 1949.

[14] Dowdeswell, R.M. and Payne, P.A. "Odour measurement using conducting polymer gas sensors and an artificial neural network decision system." Engineering Science and Education Journal. June 1999.

[15] Witten, I.H. and Frank, E. Data Mining San Fransisco: Morgan Kauffman, 2000.

[16] Goldberg, D.E Genetic Algorithms in Search, Optimization and Machine Learning. Reading, MA: Addison-Wesley, 1989.

[17] Kermani, B.G., Schiffman S.S., and Nagle H.T. "Using Neural Networks and Genetic Algorithms to Enhance Performance in an Electronic Nose." IEEE Transactions on Biomedical Engineering: Vol. 46, No. 4. April 1999.

Chapter 2. Sensor Chambers

The sensor chamber of an electronic nose is part of the sample handling system and as such it must be treated with as much care as the rest of the system. A sensor chamber is not simply a box to hold the sensors. It is an integral part of the system. The sensor chamber must be designed to effectively deliver the odorant to the sensor. If the chamber contains more than one sensor, then the timing of the delivery must be controlled so that the odorant is delivered to each sensor simultaneously. Since the chamber is part of the sample handling system, overall volume must be minimized. In many applications, only small amounts of odorant material will be available. Therefore, low dead volume in the sampling handling system must be a design criterion.

2.1 Design Considerations

Several factors must be taken into consideration when designing a sensor chamber for an electronic nose. Materials must be selected that generate structural integrity-while minimizing interactions with the odorant molecules. The sensor substrates and interconnects are also important, because the sensors become an integral part of the sensor chamber. In some cases, the sensors are designed and manufactured specifically to be part of the sensor chamber.

2.1.1 Chamber Materials

The materials that are used in sensor chambers must be selected with care. Certain materials can retain and/or react with the odorant molecules and produce undesirable byproducts. If the material of which a sensor chamber is made can easily retain odors, then an obvious memory effect will occur. Generally, stainless steel has been used in the past because of its convenience and commercial availability, as well as its resistance to chemical interactions. Another material that has been used in electronic nose environments is Teflon. Although it is thought to be micro-porous and therefore may retain odors, its chemical inertness and its desirable machining properties has made it a material of choice in the research environment.

2.1.2 Sensor Substrates and Interconnect

The sensor chamber must be appropriately designed to accommodate the sensors while meeting the system requirements for sample delivery and electrical connectivity. The sensors must be placed in the chamber in such a way that the air sample containing the odorant molecules is delivered from the sample source directly onto the sensor surface to enhance sensor response.

Sensors should be designed with the connectivity in mind. Often, the connection pads of the sensor are made of a precious metal like gold using thin-film deposition processes. Since soldering on gold is not an option, another alternative mechanism is necessary. A Zero Insertion Force (ZIF) connector is a good alternative for connectivity, but the ZIF connector applies a limited amount of force to the connection area. Thus, the gold connections pads must be thick enough to withstand the pressure of the ZIF connector. The material of which the ZIF connector is made can also hold odors. Hence, the chamber design should ensure that the connectors themselves be isolated from the odorant flow path.

A design alternative that meets this objective is a configuration that positions the sensor so that the part of the sensor substrate that must be connected protrudes through the chamber wall. This will eliminate the concern about the connector material holding odors, but will introduce a new concern about sealing the chamber around the sensors substrates.

The chamber must be sealed but the electrical connection must be maintained. Either the wires from the connectors must pass through the chamber wall or part of the sensors substrates must protrude through the chamber wall.

2.2 NC State E-Nose Sensor Chamber Analysis

The E-Nose at NC State, in its current configuration, has two sensor chambers. One is made of stainless steel and the other is made of Teflon®. The focus of the work presented here is the design of a new Teflon® sensor chamber.

2.2.1 NC State E-Nose Hardware Configuration

The NC State E-Nose basically consists of a 12-sample auto-sampler, a Teflon® conducting polymer sensor chamber, a stainless steel MOS sensor chamber, a mass flow controller, an air pump, and a LabVIEW® control program. A diagram of the NCSU E-Nose is shown in Figure 2.1.

The odorants being sampled are drawn through the system using the pump at the exhaust outlet and the flow is controlled using the mass flow controller. The sensor response is measured and amplified by analog circuitry and is then fed into a computer via a National Instruments AT-MIO16 interface board.

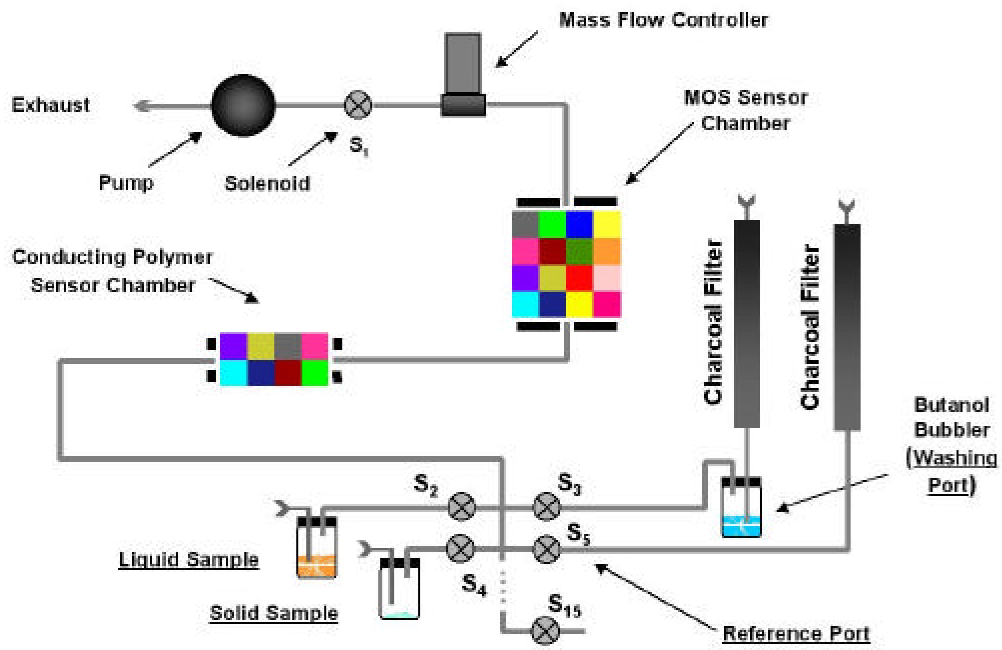

Figure 2.1 NCSU E-Nose Hardware

A LabVIEW® program samples the E-nose response once each second and logs the data into a spreadsheet file. The spreadsheet file can then be analyed using a Matlab® program.

The MOS sensor chamber was precision machined from stainless steel and can house up to 16 gas sensors in a standard TO-5 package. Currently it is populated with commercial metal-oxide Taguchi® (TGS) and Capteur® gas sensors. The chamber was designed so that the gas can be jetted directly onto the sensor surface to improve sensitivity and response time. A drawing of the chamber is shown in Figure 2.2.

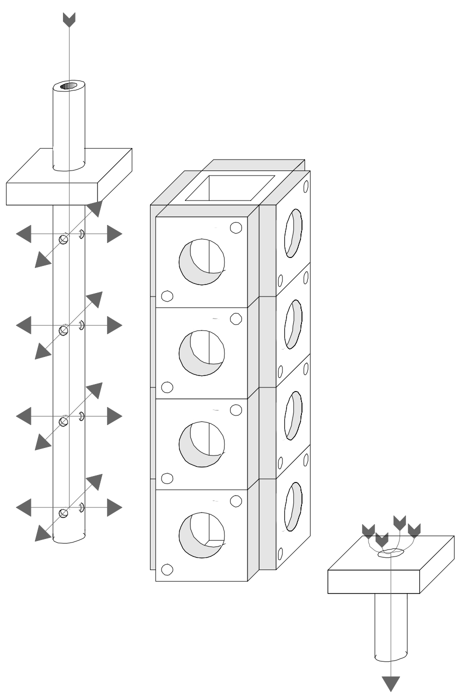

Figure 2.2 MOS sensor chamber drawing

Figure 2.3 MOS sensor chamber photo

As you can see in the photograph of Figure 2.3, a small circuit board is used as an interface between four of the MOS sensors and the ribbon cable that is connected to the sensing circuit.

The Conducting Polymer sensor chamber was machined from Teflon® and can house up to four sensors. Photographs of the sensor chamber are shown in Figures 2.4 and 2.5.

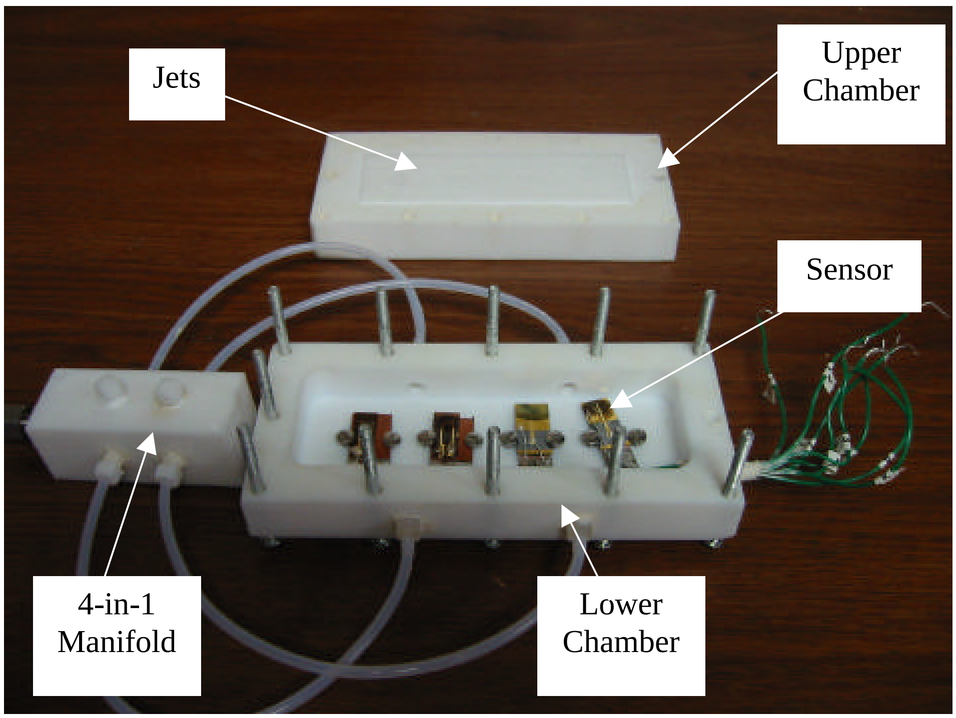

Figure 2.4 Conducting polymer sensor chamber

As shown in Figure 2.4, the conducting polymer sensor chamber was manufactured using two blocks of Teflon®. The upper chamber houses the main gas inlet and the twelve distributed gas jets. The lower chamber houses the four gas outlets and the four conducting polymer sensors. A magnified view of the sensors in the chamber is shown in Figure 2.5. In the photograph in Figure 2.5, note that the conducting polymer sensors are fastened to the bottom of the sensor chamber using stainless steel screws.

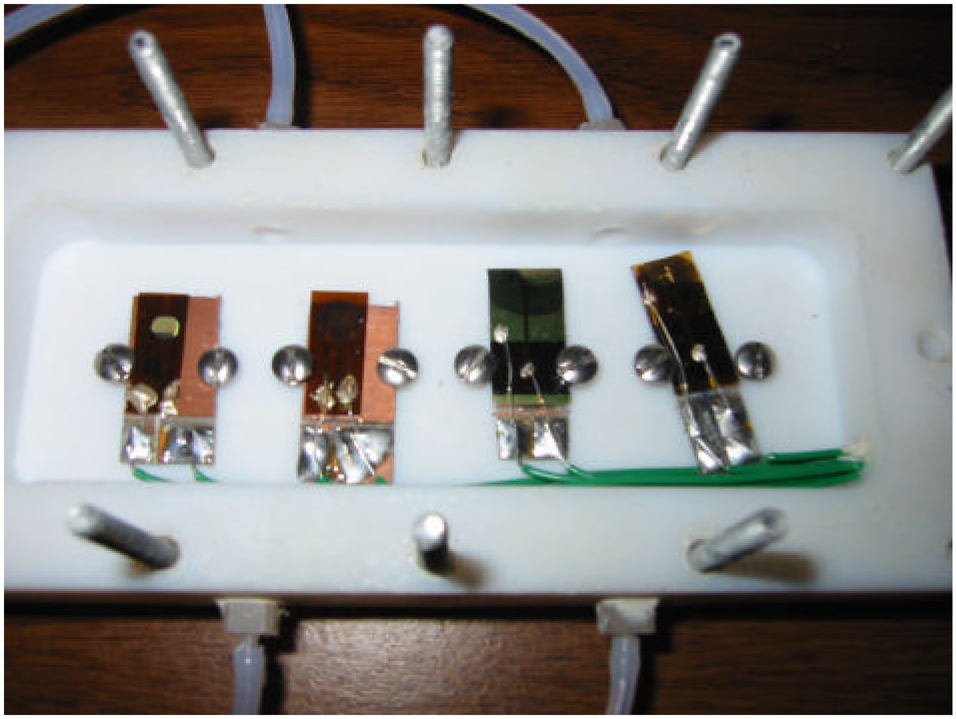

Figure 2.5 Sensors in conducting polymer sensor chamber

2.2.2 Finite Element Analysis of Conducting Polymer Sensor Chamber

The response of a sensor is directly proportional to the concentration of odorant molecules that are transported to the sensor's surface. Consequently, the fluid flow characteristics of the chamber are an important factor in establishing system sensitivity. We examined the fluid flow characteristics of the existing conducting polymer sensor chamber using ANSYS® software. The model for the interior volume of the chamber was built using the ANSYS® graphical user interface and a finite element mesh was mapped onto the volume model. Finite element analysis was then performed using flow rate settings of 1 liter per minute. The interior volume model is shown in Figure 2.6.

There is one inlet and four outlets to the chamber. The sensors are on the bottom of the chamber. The gas flows in the inlet at the top end of the chamber and is delivered through twelve openings in the top of the chamber. The four sets of the three inlets are evenly spaced so that each set of inlets is directly above a sensor. The gas flows out from each side of the chamber. The volume of this chamber is 3.27 cubic inches. The finite element mesh is shown in Figure 2.7.

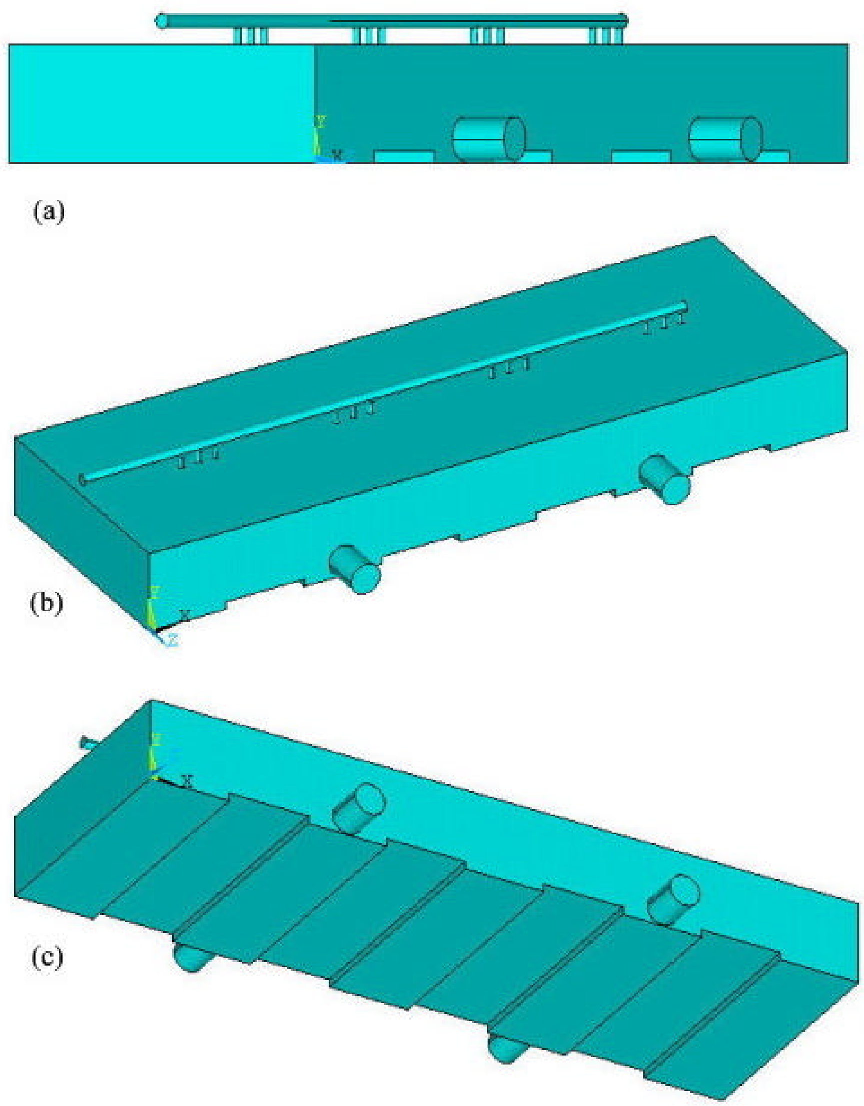

Figure 2.6 Interior volume model of conducting polymer sensor chamber (a) side view; (b) top view; (c) bottom view.

The finite element mesh was created by using eight divisions per inch on each of straight lines and by using an arbitrarily larger number of divisions per inch for the cylindrical volumes in the chamber. Tetrahedral elements were used. Velocity loads of zero velocity were applied to all areas of the model. This created the boundary conditions. The loads were then changed so that an inlet velocity of 331 inches/second and an outlet velocity of 9.2 inches/second were applied. These velocities correspond to a flow rate of 1 liter per minute, which is in the range that we operate the electronic nose.

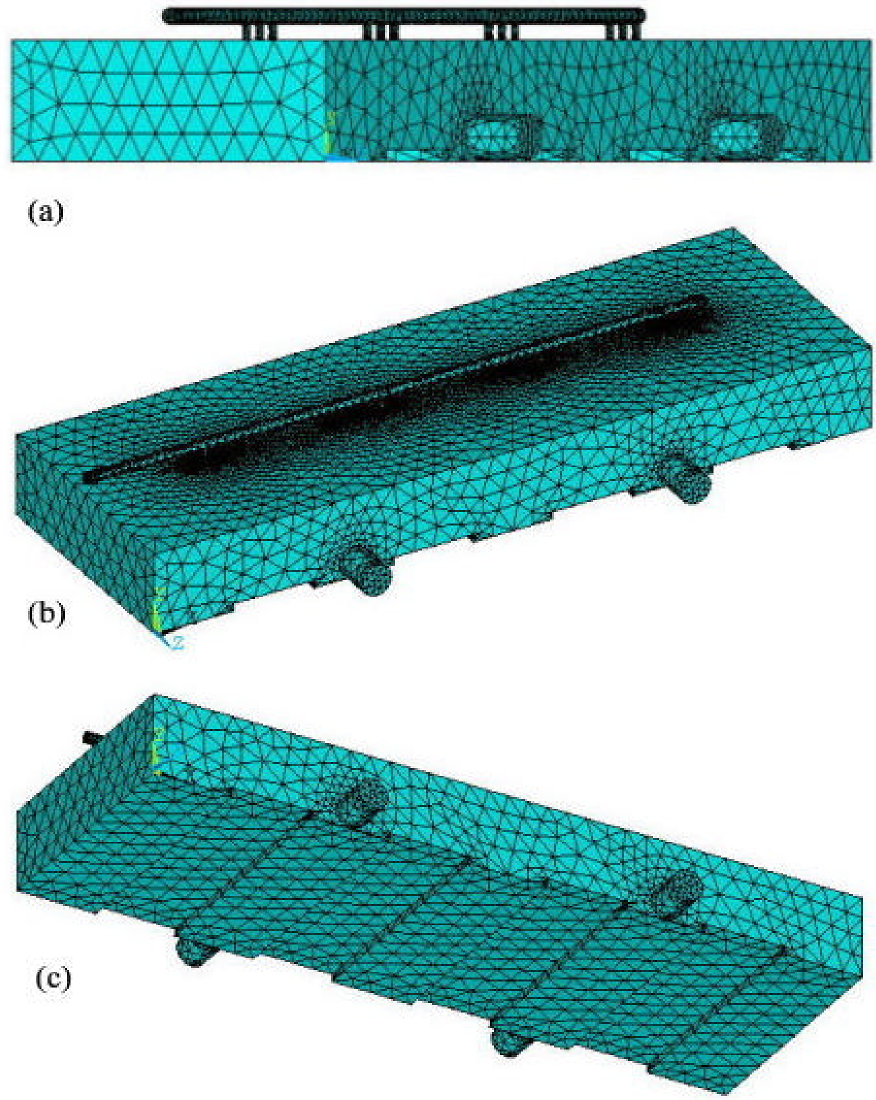

Figure 2.7 Finite element mesh of conducting polymer sensor chamber (a) side view; (b) top view; (c) bottom view.

The simulation results are shown in Figure 2.8.

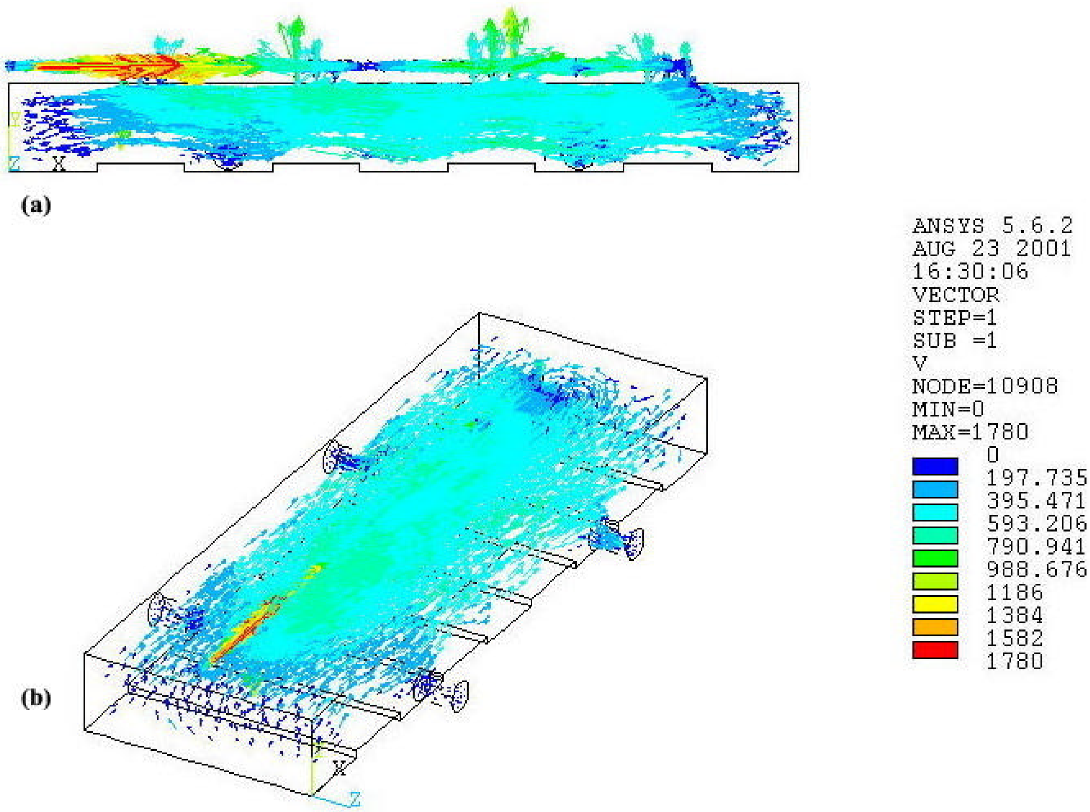

Figure 2.8 Flotran simulation results for original conducting polymer sensor chamber.

As you can see from the simulation results, the high velocity at the inlets decreases when it reaches the first set of jets. The velocity in the rest of the chamber is consistent. What is desirable are high velocity odorant streams flowing from the inlet jets down onto the sensors. These were not obtained. An illustration is shown in Figure 2.9.

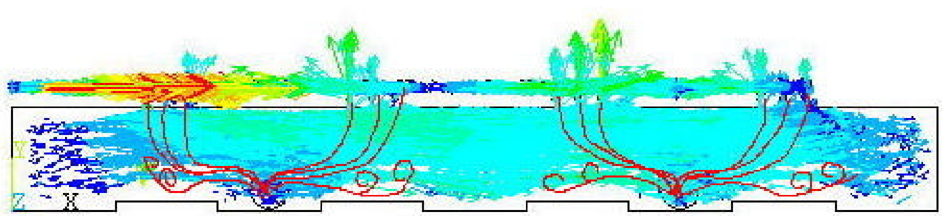

Figure 2.9 Desired turbulence in conducting polymer sensor chamber

2.2.3 Improvements to Current Design

Several deficiencies may be noted in the existing sensor chamber design. First, there is an excessive amount of dead volume in the chamber. Second, the desired turbulent flow in the odorant streams has not been achieved. Third, the timing of arrival of the odorant to each individual sensor is not the same. These qualities are desirable in sensor chamber design.

As for the excessive dead volume, if the total volume of the odorant delivery system is greater than the headspace of the odorant of interest, then the headspace will get depleted before the sensor analysis is finished. To avoid this, either the volume of the odorant delivery system must be reduced, or a constant regeneration of the headspace must occur. Generally, the least amount of volume should be used. The first improvement that can be made to the chamber is to reduce its volume.

The second issue to be dealt with is the laminar flow of the odorant streams as they are delivered to the sensors. Ideally, turbulent flow is desired so that all of the odorant reaches the sensor surface. If the flow at the sensor surface is laminar, the opportunity for odorant - sensor interaction is decreased.

The third issue is the timing of the odorant to the individual sensors. The velocity of the odorant streams should be controlled so that the odorant is delivered to each of the sensors at the same time. This can be accomplished in several ways. If we were to use a sensor chamber with the same configuration as the one that current chamber, then the way to control the velocity of the odorant streams is to use flow-channel contractions and expansions. By using sudden expansions and sudden contractions of the inlet and outlet pipes, and using the appropriate dimensions, the velocity of the gas streams and the timing of the odorant can be controlled such that the odorant reaches each sensor simultaneously. Using the Bernoulli continuity equation, $A_1V_1 = A_2V_2$, the appropriate sizes of the expansions and contractions were calculated. An example design of the improved sensor chamber configured with the sensors in the same position as the existing chamber is presented in Figure 2.10 (interior volume model). In the improved design, the volume has been dramatically reduced and the number of inlet jets has been reduced from four sets of three to four individual jets, and the timing of the odorant has been improved.

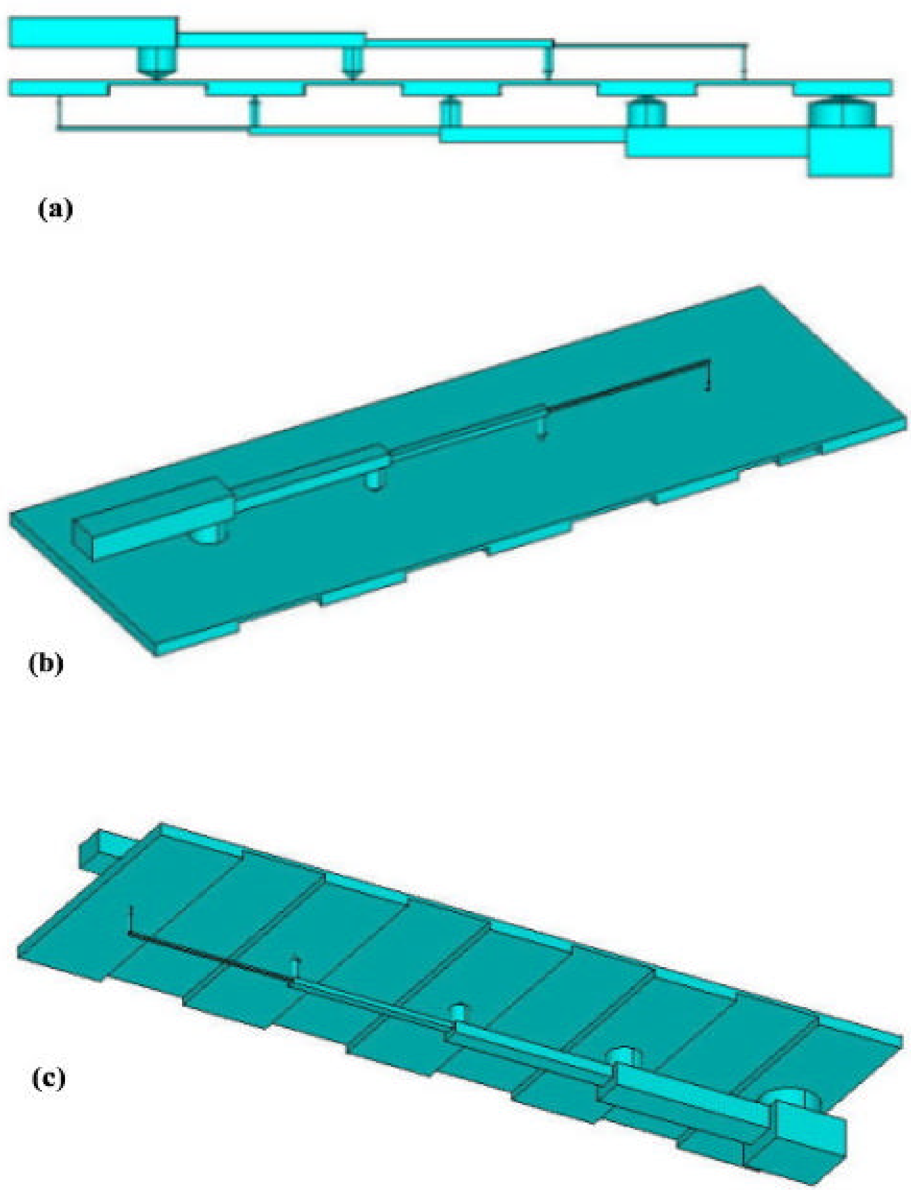

Figure 2.10 Suggested improvements to conducting polymer sensor chamber (a) side view; (b) top view; (c) bottom view.

2.2.4 **Limitations of the Proposed Improvements**

There are several limitations to this new design (see Tables 1 and 2). First, due to the length of the sensor chamber, very large cross-sectional areas had to be used to get the desired velocities. Second, the smallest inlet pipe (4.75 in. long and 0.016 in. diameter) is so small that it would be difficult to drill in one block of Teflon®. Thus, manufacturability becomes an issue. By designing another configuration for sensor chamber, these limitations can be avoided.

Table 1. Chamber Inlet Specifications

Segment	Area (square inches)	Velocity (inches/second)	Length (inches)	Diameter (inches)
1	$0.2*10^{-3}$	1270	1.112	0.016
2	$1.99*10^{-3}$	128	0.112	0.05
3	$1.65*10^{-3}$	307	1	0.045
4	$9.37*10^{-3}$	27.1	0.112	0.109
5	$7.81*10^{-3}$	97.6	1	0.998
6	$32.6*10^{-3}$	7.79	0.112	0.204
7	$27.2*10^{-3}$	37.4	0.75	0.186

Table 2. Chamber Outlet Specifications

Segment	Area (square inches)	Velocity (inches/second)	Length (inches)	Diameter (inches)
1	$0.2*10^{-3}$	1020	1.112	0.016
2	$1.99*10^{-3}$	102	0.112	0.05
3	$1.65*10^{-3}$	246	1	0.045
4	$9.37*10^{-3}$	21.7	0.112	0.109
5	$7.81*10^{-3}$	78.1	1	0.998
6	$32.6*10^{-3}$	6.24	0.112	0.204
7	$27.2*10^{-3}$	29.9	1	0.186
8	$93.3*10^{-3}$	2.18	0.112	0.344
9	$77.7*10^{-3}$	13.1	0.75	0.314

2.3 New Conducting Polymer Sensor Chamber Design

A new radial flow sensor chamber is proposed. This sensor chamber will have several radial channels that will deliver the odorant in unison to individual sensor chambers. The sensors are positioned in an arc with each sensor being equidistant from the inlet source. Since each channel has equal length, the concern about timing the delivery of the odorant to each sensor is eliminated. Two alternatives for the chambers have been examined.

2.3.1 First Alternative

The first alternative, shown in figure 2.11, has gas inlets on top of the sensors and outlets on the bottom. The sensors are positioned horizontally. As can be seen in Figure 2.11, the odorant streams are directed through the radial channels into each individual sensor chamber and onto the top of each sensor. The odorant is removed from the chamber from underneath the sensor. The odorant will reach each sensor at approximately the same time. A finite element mesh of the individual sensor chamber is shown in Figure 2.12. There are more elements on the top of the model than on the bottom. This is because more accuracy in the simulation was desired above the sensor surface. The simulation results are shown in Figure 2.13.

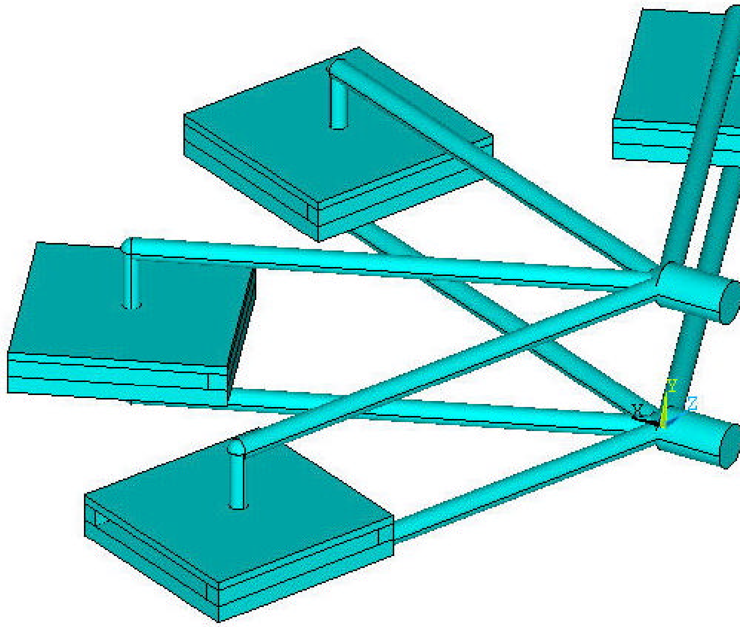

Figure 2.11 Radial flow sensor chamber – horizontal configuration

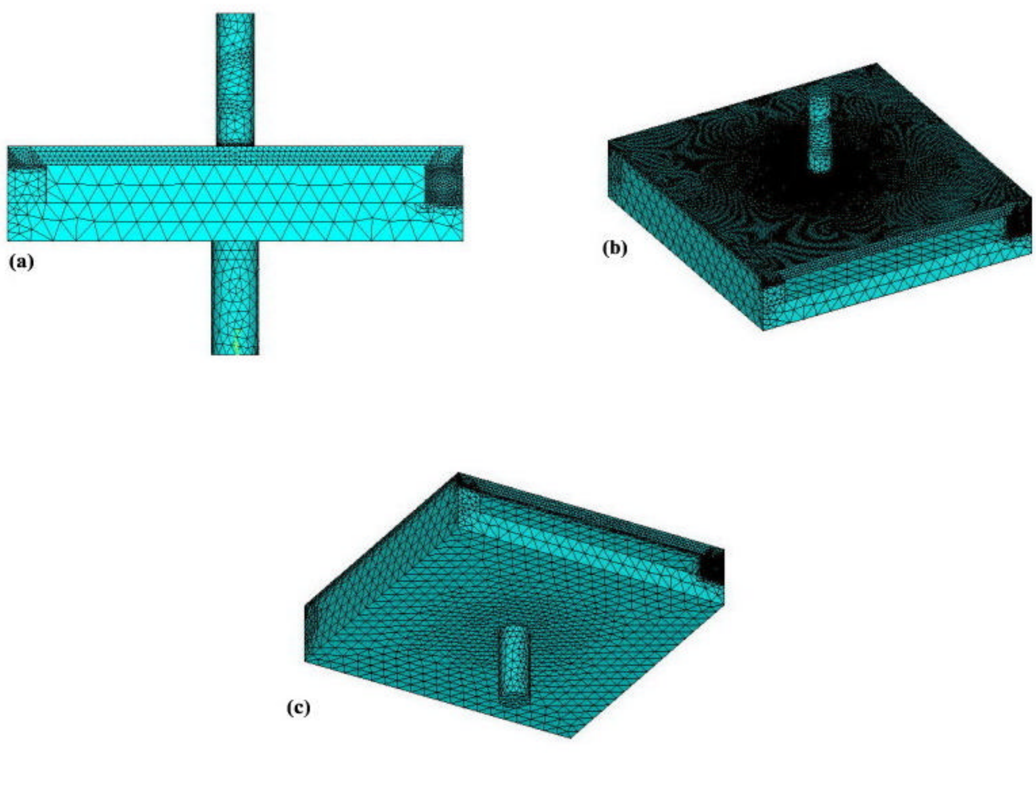

Figure 2.12 Finite element mesh of horizontal sensor chamber. (a) side; (b) top; (c) bottom.

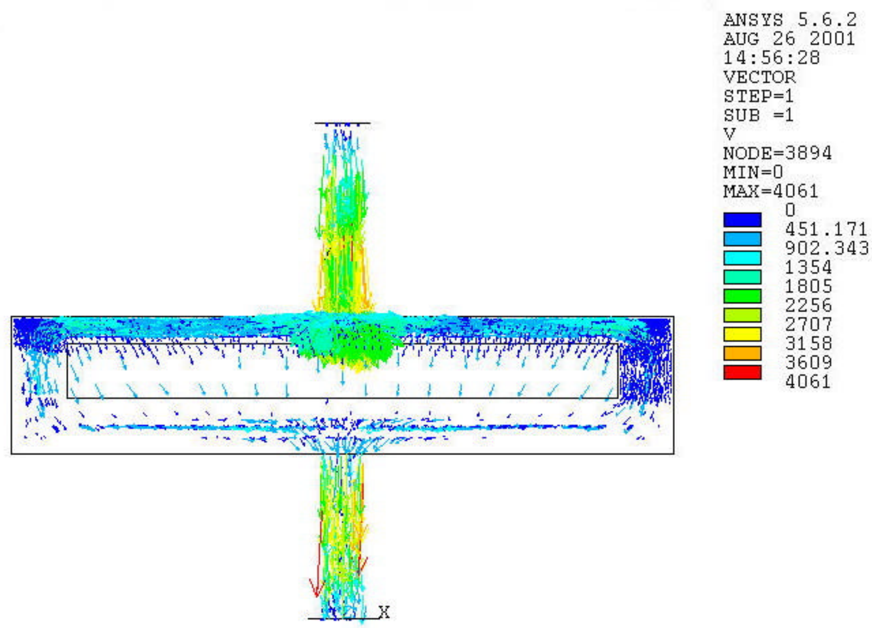

Figure 2.13 Flotran simulation results of horizontal sensor chamber

As can be seen from the simulation results in Figure 2.13, the odorant enters the chamber with a high velocity and that slows as the stream approaches the top of the sensor. At the surface, laminar (non-turbulent) flow is produced.

2.3.2 Second Alternative

The second alternative, shown in figure 2.14, has the gas inlets and outlets on the top of the sensor. The sensors are positioned vertically and the odorant streams are directed into each individual sensor chamber onto the top of each sensor.

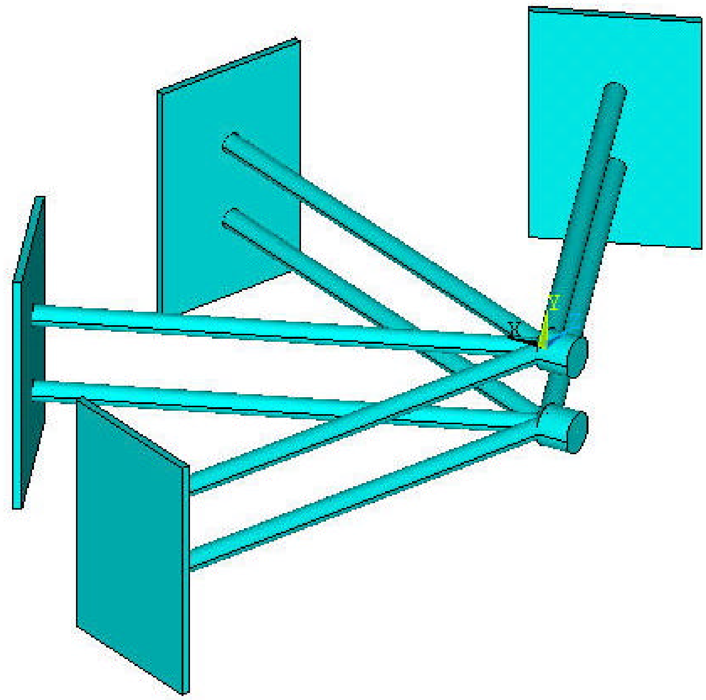

Figure 2.14 Radial flow sensor chamber – vertical configuration

The odorant is removed from the chamber from the top of the sensor substrate. In this configuration, the sensor substrate forms the back wall of the chamber. As with the first alternative design, the odorant will reach each sensor at approximately the same time. The analysis of an individual channel follows. The volume model of the individual channel is shown in Figure 2.15.

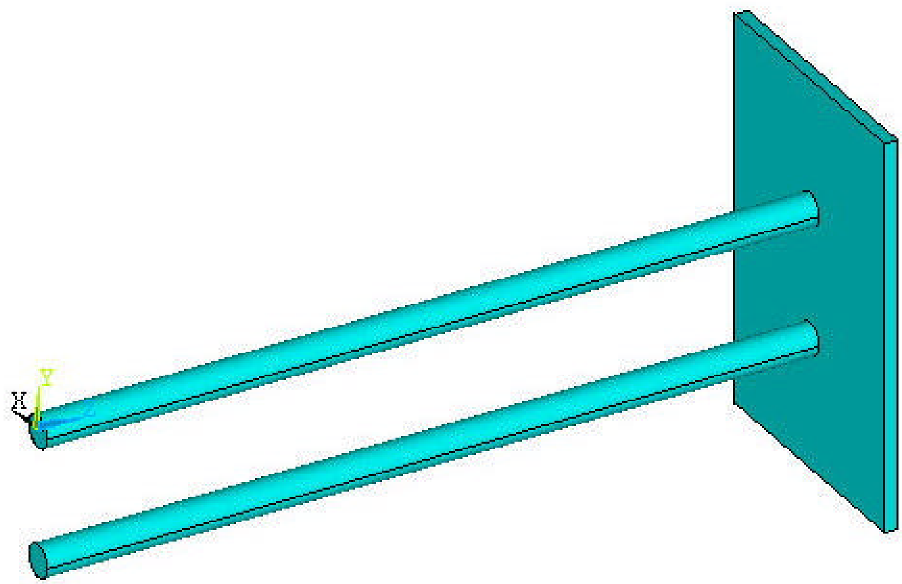

Figure 2.15 Volume model of vertical sensor chamber

The finite element mesh of the vertical sensor chamber is shown in Figure 2.16. Note that there are more elements near the end of the chamber where the sensor is located. As always the number of elements should be increased at the area of interest to improve the resolution of the simulation results. The simulation results are shown in Figure 2.17 and Figure 2.18.

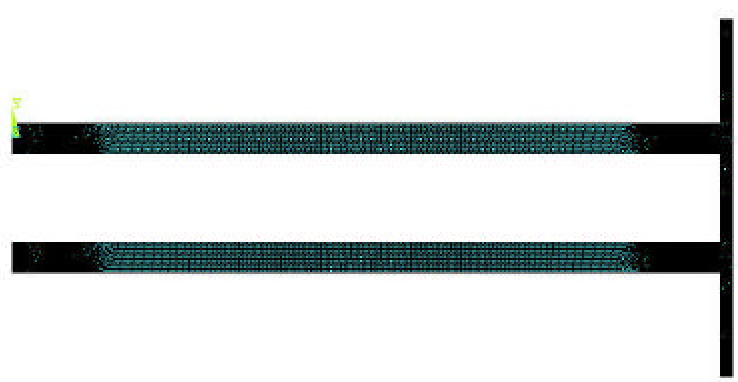

Figure 2.16 Finite element mesh of vertical sensor chamber

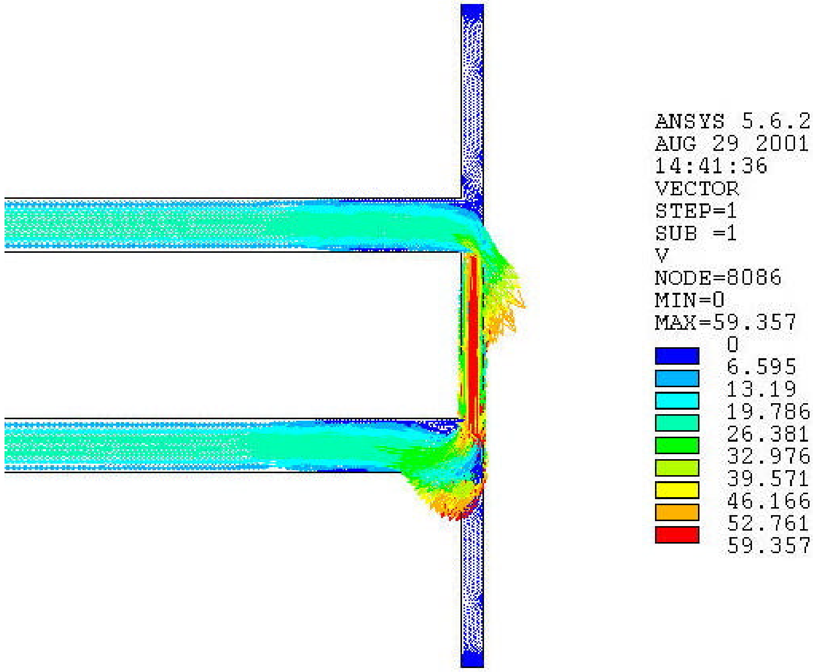

Figure 2.17 Flotran simulation results of vertical sensor chamber I

As can be seen in Figure 2.17, there is laminar flow throughout the sensor chamber with what appears to be odorant collisions at the sensor surface.

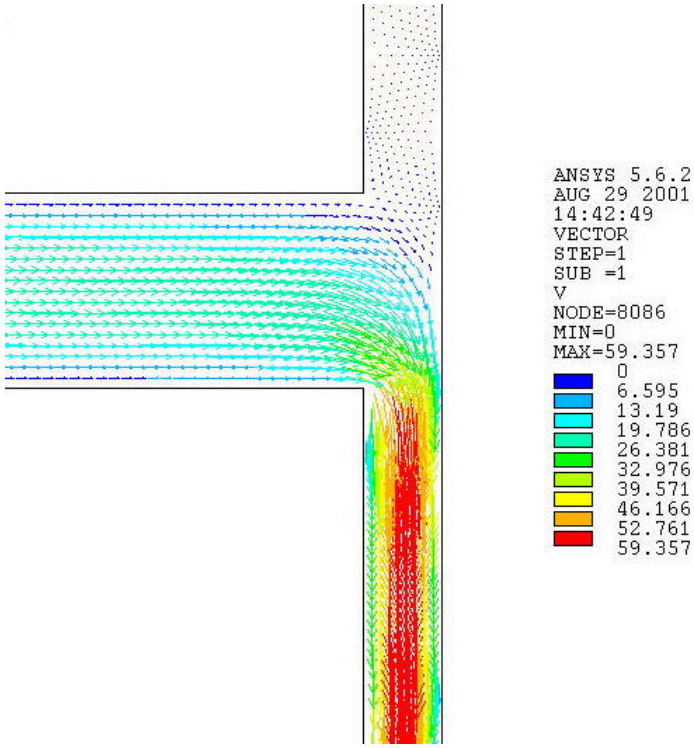

Figure 2.18 Flotran simulation results of vertical sensor chamber II

But, as shown in Figure 2.18, the collisions do not really exist. They appear in the first figure because the magnitudes of the velocity vectors at those locations are so much stronger than all the other velocity vectors in the sensor chamber. By increasing the magnification of the software in the region of interest, a laminar high velocity odorant stream is observed.

2.3.3 Turbulence

Both of the proposed alternative designs solve two problems that exist with the existing conducting polymer sensor chamber. They both have low dead volume and appropriately time the delivery of odorant to each sensor. The problem that they do not solve is that of turbulence.

Generating the turbulence desired in the sensor chamber could not be achieved easily. The typical measure of turbulence in a system is the Reynolds number. Its equation is given as $R_e = \frac{V \cdot d \cdot r}{m}$, where V = the velocity of the fluid, d = the diameter of the pipe, r = the density of the fluid, and μ = the dynamic viscosity. The appropriate Reynolds number to achieve turbulence is generally accepted to be at or about 2000. The Reynolds number for the alternative designs is in the 200 to 300 range. The limiting factor in our design is the velocity of the fluid. If the velocity of the fluid is greatly increased, the headspace of the odorant will be completely depleted before the sensor has completely responded in some applications.

An option would be to change the geometries of the chamber in such a way that eddies and vortices could be generated to achieve the appropriate turbulent flow. Several geometric configurations designed to implement this ideas were simulated using the ANSYS® Flotran software, but none were successful. Because of the difficulty in generating the desired turbulence in the sensor chamber, a new approach is proposed that is not dependent on turbulence.

2.3.4 New Hardware Configuration

A “sniff and hold” mode is proposed to compensate for the lack of turbulence in the sensor chamber. If cutoff valves are used at both ends of the sensor chamber, the odorant can be drawn into the chamber and then the chamber can be sealed off using the valves. In this mode, diffusion mechanisms will dominate and the odorant can interact with the sensors without the continuous laminar flow of gas to interfere. A diagram of the new hardware configuration is shown in Figure 2.19.

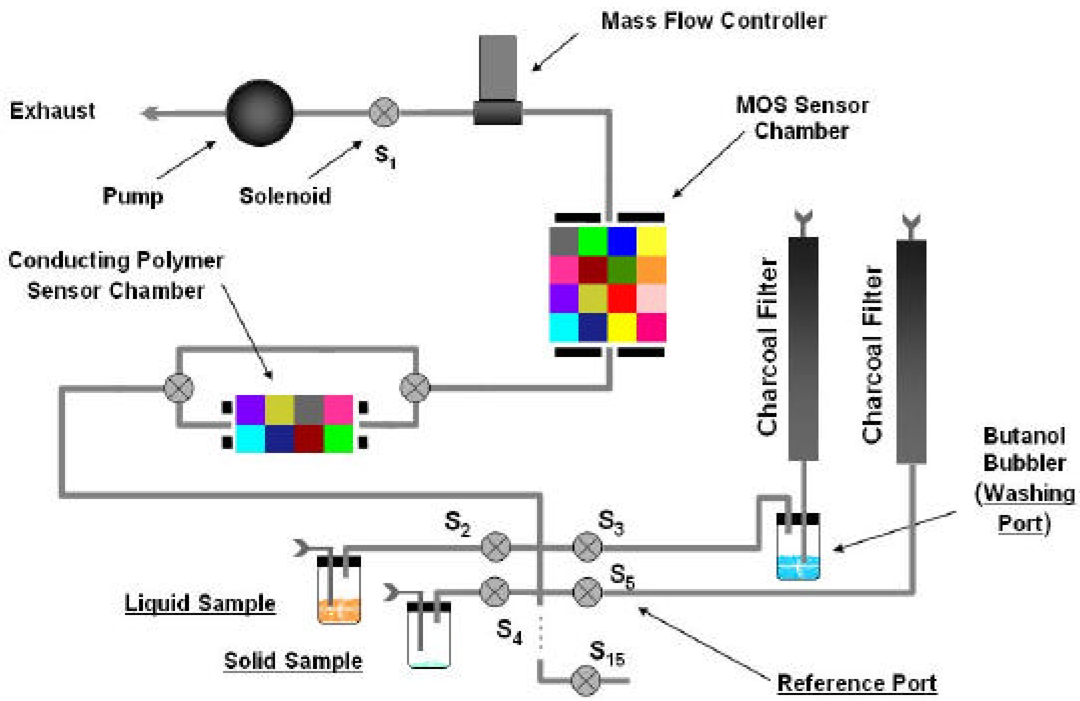

Figure 2.19 NC State E-Nose "sniff and hold" configuration

2.4 Experimental Results

A new sensor chamber using the second alternative design was built and tested with four conducting polymer sensors. Tests were conducted using a continuous laminar flow and a "sniff and hold" mode of operation. The final sensor chamber and the test results are detailed in this section.

2.4.1 Experimental Setup

The sensor chamber is similar to that of the second alternative design detailed in section 2.3.2. Figure 2.20 shows the sensor chamber disassembled. It can be seen from the photograph that the core of the sensor chamber is octagonal in shape and has 19 component pieces. The sensors are positioned vertically on the outside of the Teflon sensor chamber core and Teflon® caps are placed outside the sensors. Aluminum plates are placed on the outside of the Teflon® caps and help to distribute the force of the screws.

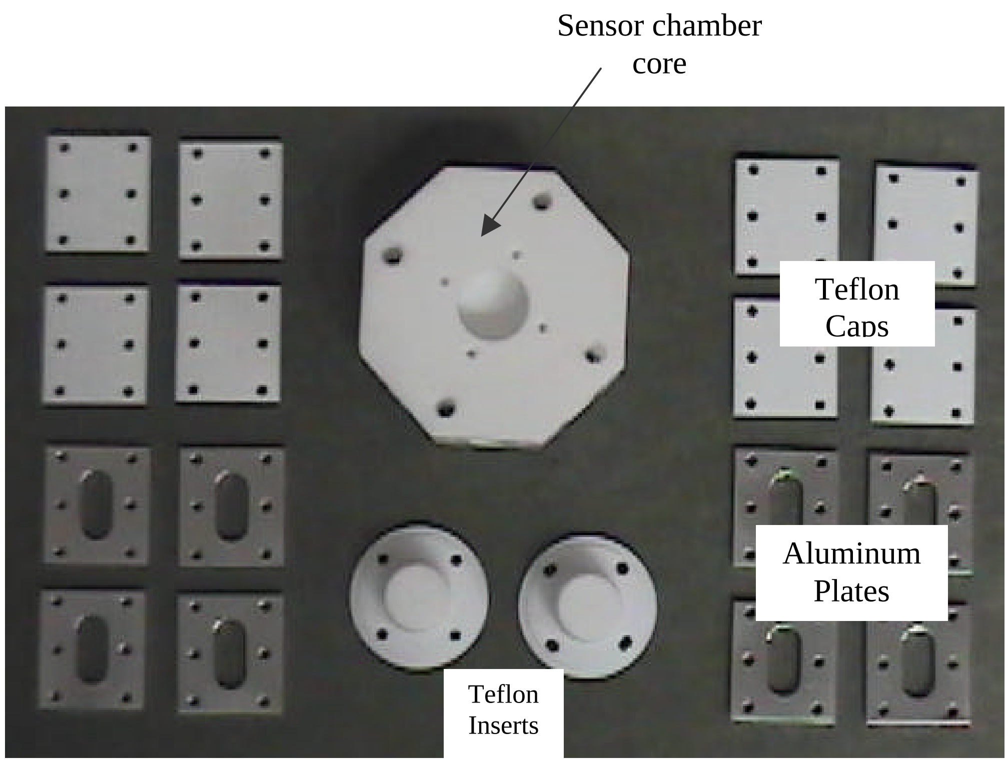

Figure 2.20 New conducting polymer sensor chamber (disassembled)

Two round Teflon® inserts are used to distribute the gas flow to each of the eight channels. A magnified view of the sensor chamber core is shown in Figure 2.21. It can be seen from that photograph that during assembly a round Teflon® insert is installed in the top of sensor chamber core. The bottom of the sensor chamber core is identical to the top and the other round Teflon® insert gets installed into the bottom of the sensor chamber core. On each of the octagonal sides of the sensor chamber core, the inlet and outlet gas channels can be seen. The fully assembled sensor chamber (without sensors) is shown in Figure 2.22. The sensor chamber is connected to the sample handling system via flexible Teflon® tubing.

Figure 2.21 New conducting polymer sensor chamber (core)

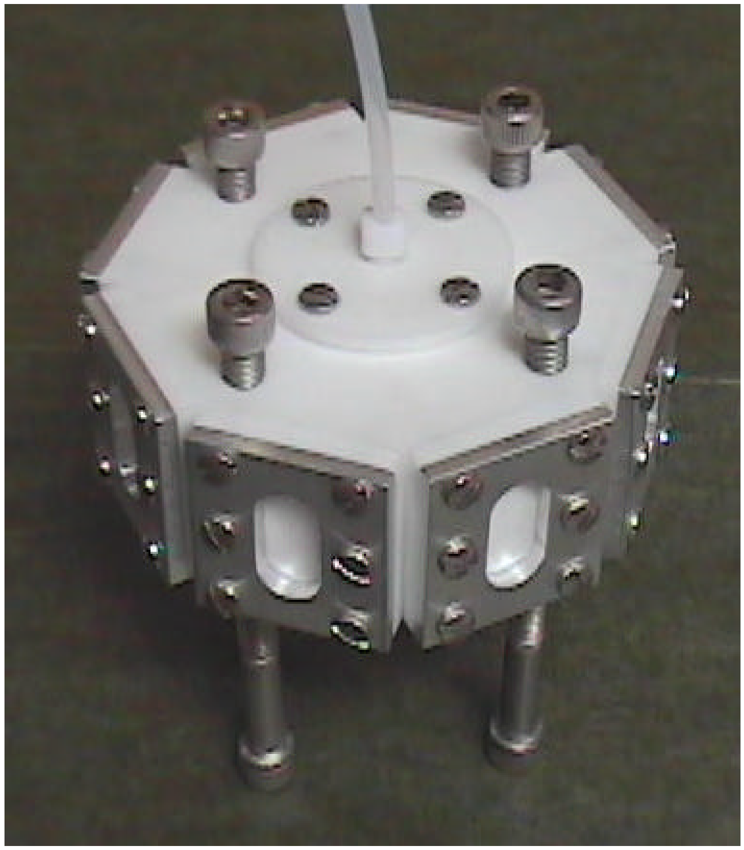

Figure 2.22 New conducting polymer sensor chamber (assembled)

The conducting polymer sensors are microfabricated using a flat, 3-mil Kapton® substrate. These flat-form sensors are placed over the center holes in the sides of the Teflon® block of Figure 2.21. Then the Teflon® squares and Stainless steel caps of Figure 2.20 are used to secure the sensors in place. The conducting polymer sensors are connected to the E-Nose via a custom interface cable made from heat seal tape, a ribbon cable, and a small interface board. The custom interface cable and fully assembled chamber with sensors can be seen in Figure 2.23

Of the four conducting polymer sensors used in this experiment, two were polypyrrole sensors and two were chloroform based sensors. Dr. Krishna Persaud at the

University of Manchester Institute of Science and Technology (UMIST) is a pioneer in E-nose technology [1]. His research group supplied us with one sensor type used in this project, a new polymer dissolved in chloroform and dispensed onto an interdigitated electrode array [2]. The second sensor type is based on electroplated polypyrrole materials. These sensors were provided by Sridhar Kashyap [2]. Sensors 1 and 2 are the polypyrrole sensors and sensors 3 and 4 are the chloroform based sensors.

Four different coffees were sampled for the experiment. The four coffees were purchased from Starbucks and were Arabian, Ethiopian, Kenyan, and Columbian coffees. Twenty milliliters of each coffee was put in a jar and connected to the auto-sampler on the NC State E-Nose. Ten samples of each coffee were collected in both the continuous flow mode and the “sniff and hold” mode. The sample rate was ten cycles per second and the coffees were sampled for six seconds. Reference air was then passed through the system for thirty seconds to clean out the chamber. The flow rate was set to four liters per minute.

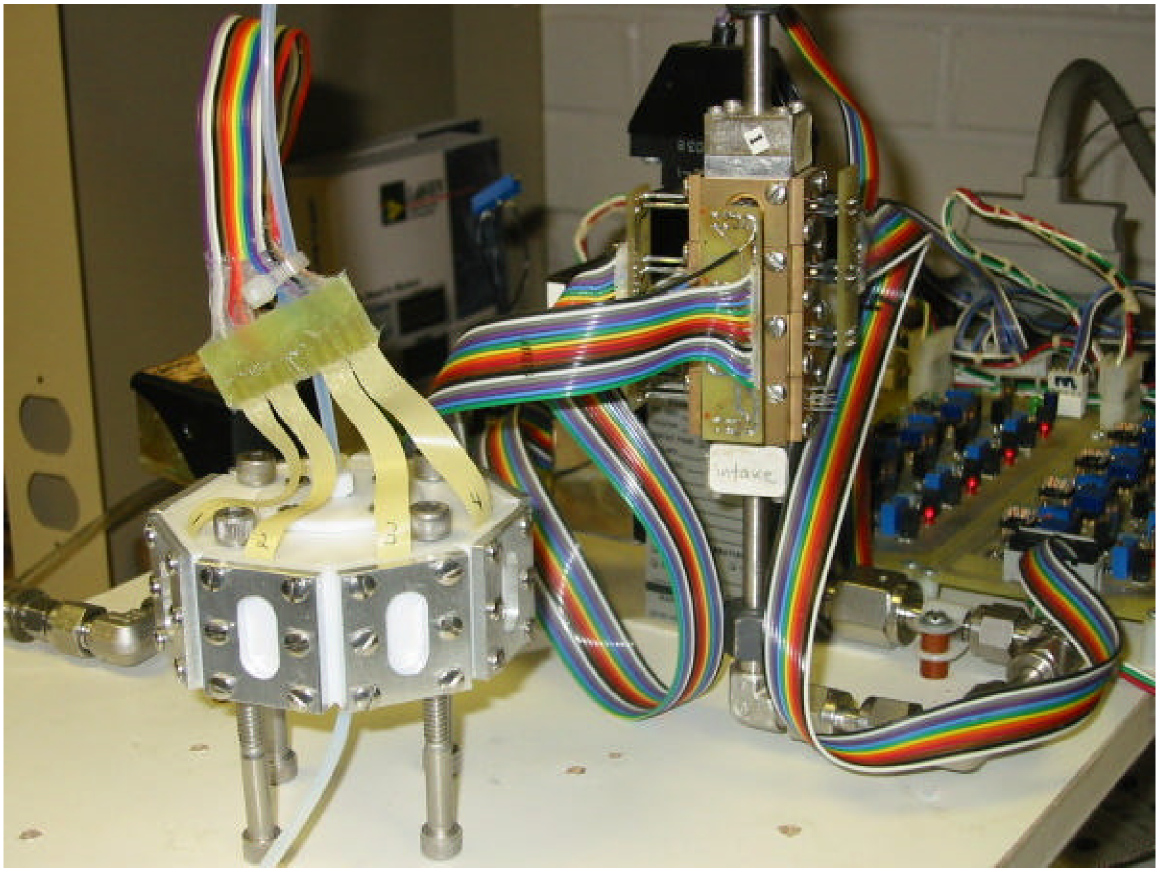

Figure 2.23 E-Nose with both sensor chambers connected

2.4.2 Test Results

The data collected from the E-Nose was analyzed using Matlab®. The average percent change in resistance was computed for each sensor, the classification rate was computed for the four sensors, and the sensor responses were plotted for evaluation. The average percent change of each sensor is shown in Table 3. The table indicates that the polypyrrole sensors responded more strongly to the continuous-flow mode of operation while the chloroform based sensors responded more strongly to the “sniff and hold” mode.

Table 3. Average percent change in resistance ($\Delta R/R$) of each sensor at a flow rate of 4.0 liters per minute

Coffee Type	Operating Mode	**Sensor 1** (ppy)	**Sensor 2** (ppy)	**Sensor 3** (chloroform)	**Sensor 4** (chloroform)
Arabia	"Sniff and hold"	5.7093	7.5165	104.5608	2.6987
	Continuous	5.8563	18.4212	9.1205	0.2297
Ethiopia	"Sniff and hold"	4.5583	4.1314	104.1464	2.5317
	Continuous	7.7056	11.7792	6.4384	0.0046
Kenya	"Sniff and hold"	1.0872	2.3246	139.9258	4.2499
	Continuous	2.8193	6.0307	85.1787	3.3121
Columbia	"Sniff and hold"	1.6829	0.3061	147.3489	4.5740
	Continuous	3.7921	2.9977	92.0856	3.4207

The classification rate was computed using a linear classifier [3]. The classification rate of the four conducting polymer sensors in the "sniff and hold" mode was 96.25%. The classification rate of the four conducting polymer sensors in the continuous flow mode was also 96.25%.

Shown in Figure 2.24 is a graph of the sensor response of one of the chloroform based sensors to the ten samples of Arabian coffee. The graph shows that the sensor has a much larger response in the "sniff and hold" mode than in the continuous flow mode. Overall, the chloroform based sensors performed much better than the polypyrrole sensors. The graphs of all the chloroform based sensor responses are in the Appendix.

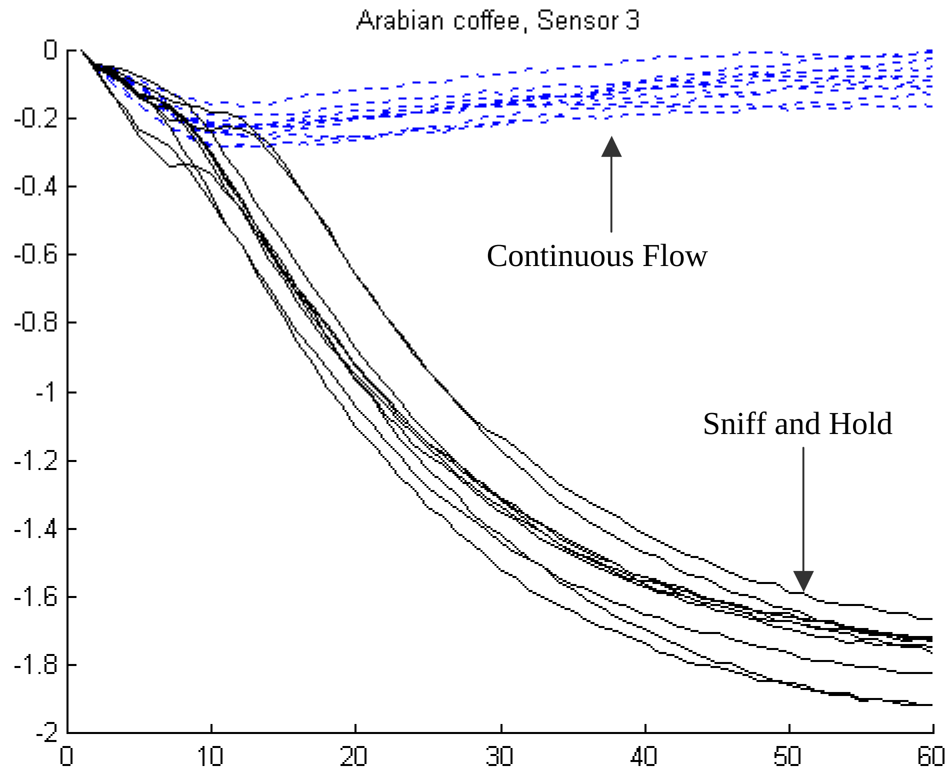

Figure 2.24 Sensor response to Arabian coffee

Further investigation has shown that the baseline resistance of the conducting polymer sensors is dependent on the flow rate of the gas flowing through the chamber. This feature of these sensors may contribute to the sensor response that is shown in Figure 2.24. A graph showing the change in E-Nose output voltage for the conducting polymer sensors at different purging-gas flow rates is shown in Figure 2.25. The sensor chamber was operated at flow rates ranging from 0.02 to 4.0 liters per minute. The figure shows that most of the transition from minimum resistance to maximum resistance occurs in the range of 0.02 to 1.5 liters per minute.

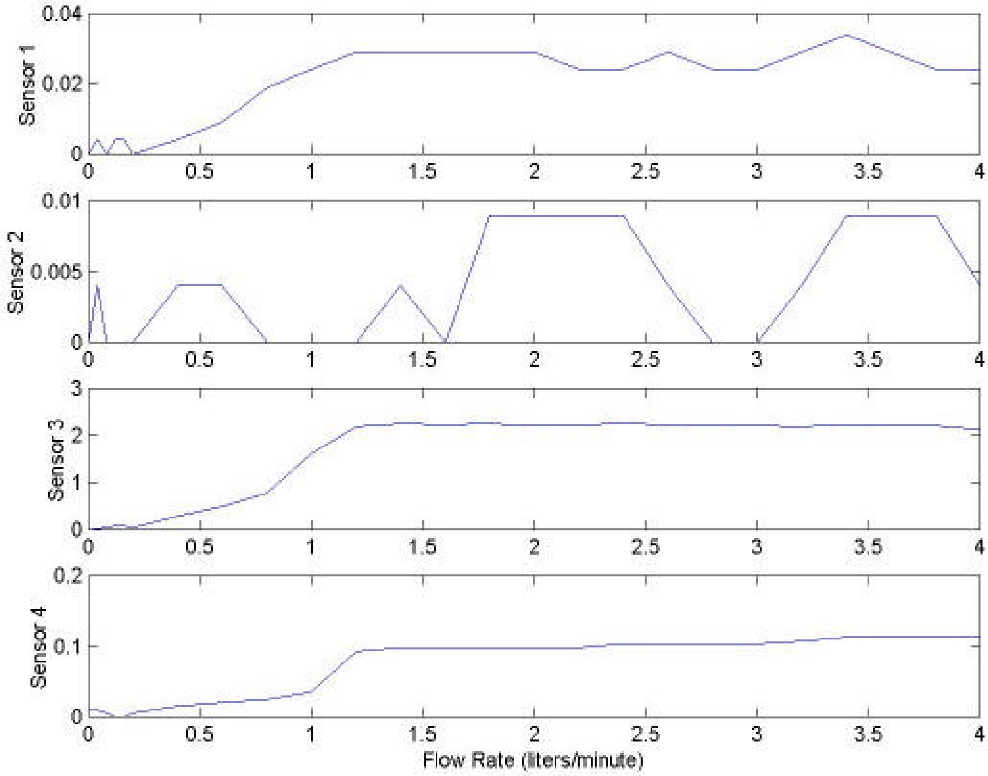

Figure 2.25 Voltage output versus flow rate

The above experiment suggests that a flow rate in the middle of the 0.02 to 1.5 liter per minute range might be more appropriate for the new conducting polymer sensors. Hence, a new test was conducted using the coffee samples. Data was collected from the E-Nose with the flow rate set to 0.8 liters per minute. The average percent change in resistance was computed for each sensor and the classification rate was computed for the four sensors. The average percent change in resistance of each sensor is shown in Table 4. For sensors 1, 3, and 4, the percent change has decreased from the results shown in Table 3. For sensor 2, the percent change has decreased for all but one coffee.

The classification rate of the four conducting polymer sensors operating at 0.8 liters per minute in the "sniff and hold" mode was 67.5%. The classification rate of the four conducting polymer sensors in the continuous flow mode was 97.5%.

Table 4. Average percent change in resistance (ΔR/R) of each sensor at a flow rate of 0.8 liters per minute

Coffee Type	Operating Mode	**Sensor 1** (ppy)	**Sensor 2** (ppy)	**Sensor 3** (chloroform)	**Sensor 4** (chloroform)
Arabia	"Sniff and hold"	2.1041	3.7334	27.4968	1.3608
	Continuous	1.5952	8.5365	17.6485	0.4694
Ethiopia	"Sniff and hold"	1.5621	2.5324	29.8026	1.4333
	Continuous	1.9154	12.1982	21.2806	0.6176
Kenya	"Sniff and hold"	0.5743	8.4914	67.7542	1.4331
	Continuous	0.6170	16.9504	61.9881	1.0378
Columbia	"Sniff and hold"	0.3805	9.3193	63.9304	1.368
	Continuous	0.9821	21.8123	66.3071	0.9848

2.5 Conclusions

The new conducting polymer sensor chamber that was built solves two problems that occurred in the existing Teflon® chamber; (1) low chamber volume, and (2) timing of the odorant to the sensors. The issue of turbulence in the new design was not resolved.

The proposed "sniff and hold" method for sampling odorants did not give better results than the continuous flow method. What is evident, however, is that for these conducting polymer sensors, the flow rate is important. The sensors were shown to be sensitive to flow rate. Therefore, when the valves were closed in the "sniff and hold" mode, an unexpected decrease in sensor response occurred. While this did not affect the classification rate at the 4.0 liters per minute operation, it did decrease the classification rate at the 0.8 liters per minute rate. These results suggest that there may actually be an ideal flow rate for each type of sensor. If such an ideal flow rate exists, then using it may result in better classification. Future work in this area is recommended.

2.6 References

[1] Courtesy Dr. Krishna Persaud (kcpersaud@umist.ac.uk, UMIST)

[2] Sridhar K.V., “Improved conductive polymer sensors for electronic nose devices,” Master’s Thesis, Electrical and Computer Engineering Department, North Carolina State University, 2001.

[3] Linnell, B.R., "The Effect of Small Samples on Statistical Pattern Recognition Techniques", Ph.D. dissertation, Electrical and Computer Engineering Department, North Carolina State University, 2001.

Chapter 3. Adaptive Interface

The analog sensor interface is an important part of any electronic nose. In many cases, the sensor response is too for the analog-to digital converter's input range. The analog interface circuit takes the sensor response and amplifies it so that it is large enough for the analog-to digital converter.

3.1 Sensor Response

Sensor response is the item of interest in all measurement systems. One problem with the NC State E-Nose is that there is no accurate record of the actual sensor resistance. With the current E-Nose configuration, the installed sensors are balanced in a Wheatstone bridge using potentiometers. For a calibration, a standard gas is "sniffed" and the gains are manually adjusted using the potentiometers. The actual gain is not known, because the potentiometers are adjusted in place in the circuit until an appropriate visual reading is obtained. Since the actual gain is unknown, the sensor resistance cannot be determined.

The actual sensor resistance gives information about the sensor and its properties over time. By using the sensor resistance changes for classification, repeatability can be attained more easily.

3.2 Sensor Drift

Sensor drift occurs with many types of gas sensors. This is commonly caused by odorant retention in the active material, humidity changes, and temperature variations. Compensation for sensor drift can be accomplished using software as described in

Chapter 1. However, drift compensation algorithms can be improved if hardware features are provided to assist in the process. As shown in Figure 3.1, sensor drift causes a DC bias in the sensor response signal. When a DC bias is present, the Analog to Digital Converter (ADC) does not operate optimally. Essentially, the ADC is wasting bits to convert the unnecessary DC bias. If the DC bias is removed within the analog circuit, before the ADC conversion occurs, then all of the bits of the ADC are being used more efficiently. In this chapter, a hardware configuration to remove this DC component is presented.

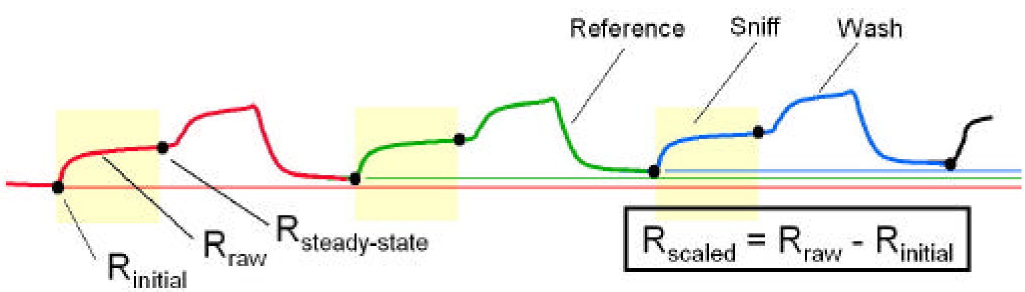

Figure 3.1 Sensor drift

3.3 Existing Sensor Interface Circuit

The existing sensor interface circuit for the NC State E-Nose is shown in Figure 3.2.

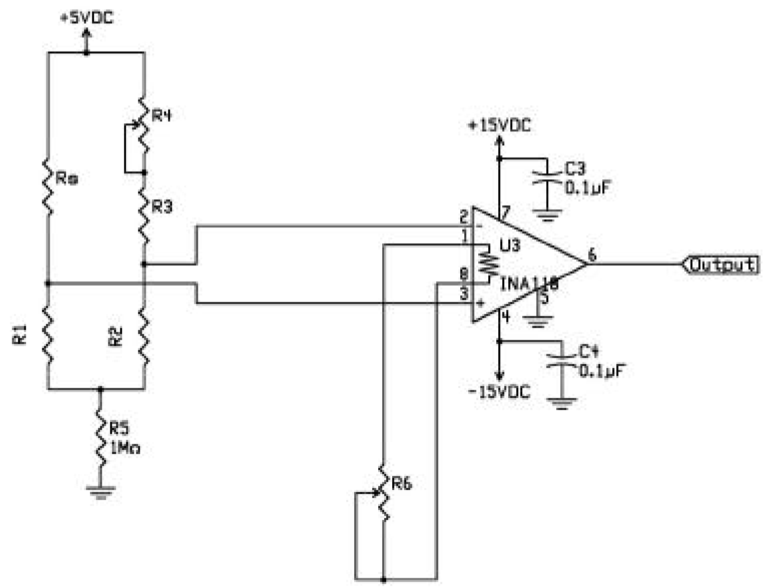

Figure 3.2 Existing sensor interface circuit

As can be seen in Figure 3.2, the sensor interface circuit that is being used consists of a Wheatstone bridge, a tail resistor to limit current, and a differential amplifier. The output of the circuit is low-pass filtered (22.6 Hz cutoff) before it is sampled by the computer. Potentiometers are being used to balance the Wheatstone bridge and to adjust the gain.

There are several disadvantages to this type of circuit. First, the output of the Wheatstone bridge is nonlinear [1]. To be run optimally, the circuit is required to operate within the linear portion of its output boundaries. Second, as a sensor drifts, the bridge becomes unbalanced and the output of the circuit will contain an altered value of DC bias. If this drifting condition persists, the operation of the circuit could drift outside its linear region. Third, manually balancing the bridge and adjusting the gain potentiometer is time consuming and can also introduce human errors. Fourth, because the gain is adjusted for an appropriate visual response, the exact gain applied to the circuit is not always known.

Due to all of these contributing factors, which are both difficult to identify, measure and isolate, the response that we get from the circuit is an overall system response. We cannot use that response and map it back to the actual sensor resistance change. To solve this problem, an adaptive interface has been designed to provide information from which the actual real-time sensor resistance can be determined.

3.4 Development of New Adaptive Interface

An adaptive interface approach was adopted in this project to compensate for sensor drift and to accurately measure sensor response. The adaptive interface has two components; (1) a sensor interface circuit and (2) a LabVIEW® control program. The key component of the sensor interface circuit is the variable resistor package. Using the variable resistor package allows the control program to adjust the balance of the bridge and the gain. Use of a linearized Wheatstone bridge ensures that the resistance-to-voltage relationship is linear by driving the sensor element at constant-current.

Using LabVIEW® to control the variable resistors, the values of the resistors are known at all times. Thereafter, LabVIEW® uses these known resistance values to compute a sensor resistance value at each sample interval. Instead of recording a system response, like a voltage or current, the actual sensor resistance profile can now be computed using circuit gain equations derived later in this section.

3.4.1 New Sensor Interface Circuit

This new sensor interface circuit shown in Fig. 3.3 contains a linearized Wheatstone bridge with an adjustable reference voltage to control the sensor current. The circuit contains four LabVIEW® controlled variable resistors labeled R1 – R4. The adjustable reference voltage (V_{ref}) is controlled with R1 and the balance of the bridge is facilitated using R2. A secondary bridge balance adjustment is available using R3 and a gain stage amplifies the sensor response. The gain stage is adjustable using R4.

The voltage output is measured by LabVIEW® using a DAQ-1200 card in a laptop computer. LabVIEW® then uses that voltage output value, the variable resistor values, and other variables such as fixed resistance values and voltage values to compute the sensor resistance. The linearized Wheatstone bridge allows us to compute a linear mapping from the voltage output to the sensor resistance.

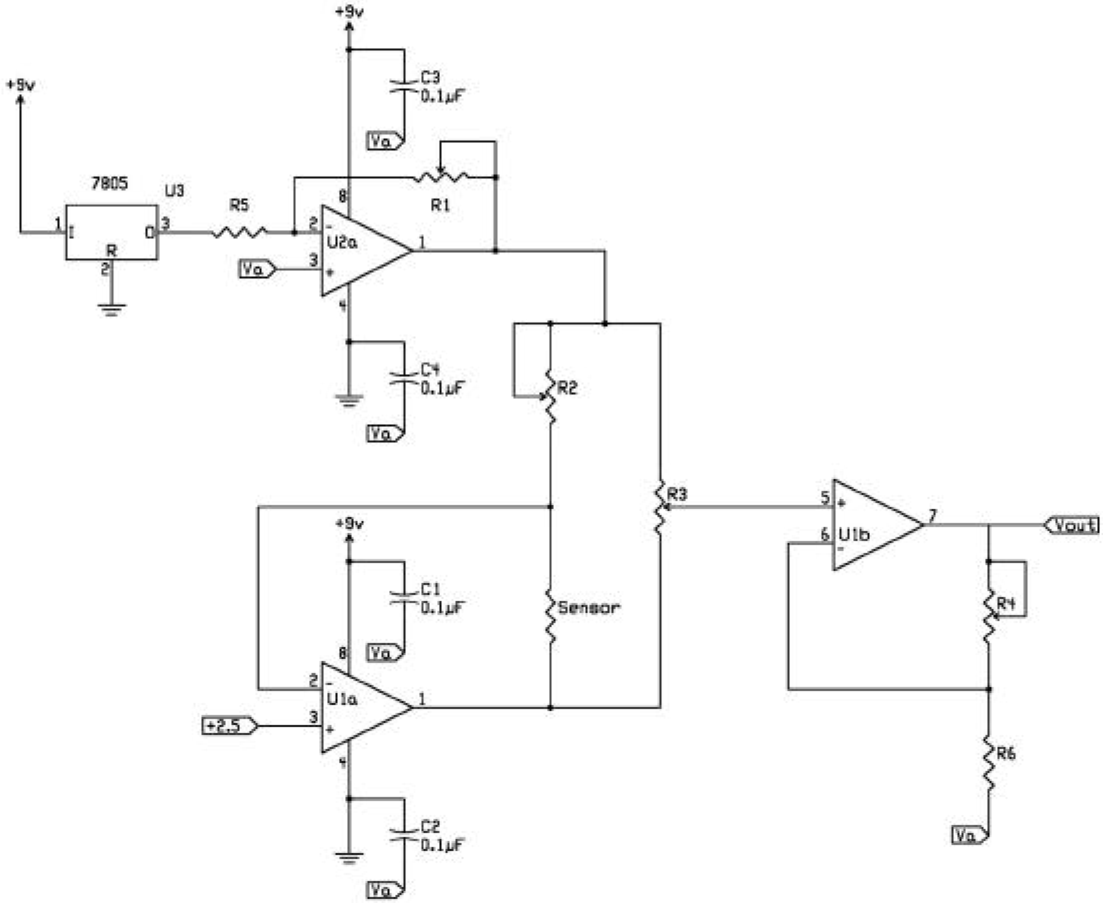

Figure 3.3 New sensor interface circuit

The circuit in Figure 3.3 is powered by a positive and negative nine volt power supply. Power for the variable resistor chip is provided by a 7805 five volt regulator. A 2.5 volt analog reference voltage V_a is used for the operational amplifiers. The AD8403 requires a power supply voltage of five volts. It does not function properly if any of the voltages applied to the variable resistors are not between zero and five volts. This mandated that the analog reference voltage be set to 2.5 volts so that the circuit would function within the required limits. The first step in understanding the output voltage of the circuit is to derive the equations for the circuit. Once the equations have been derived, it will be possible to map the sensor resistance to the output voltage.

- Circuit Equations

The linearized Wheatstone bridge portion of the circuit is repeated in Figure 3.4.

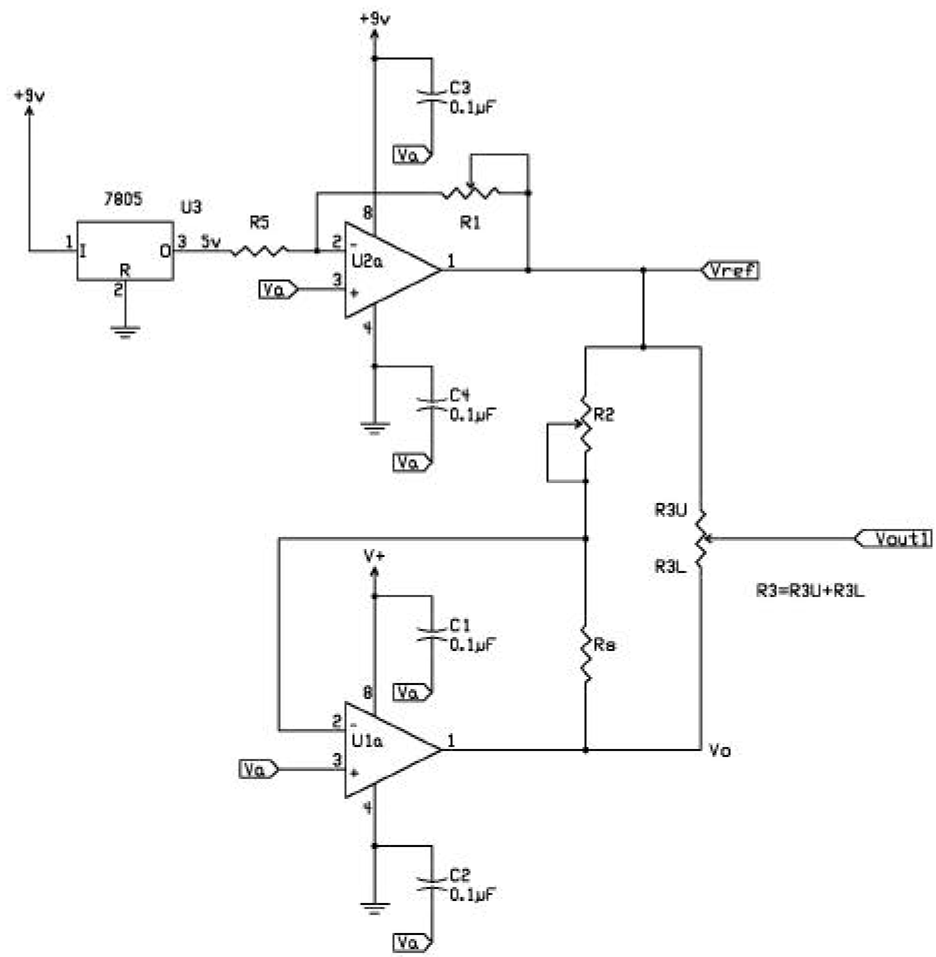

Figure 3.4 Linearized Wheatstone bridge

From Figure 3.4, the voltage output of the linearized Wheatstone bridge, $V_{out1,}$ has been defined in terms of the appropriate resistance values and the voltage references, V_{ref} and A_{ref}. The voltage reference, $V_{ref,}$ is then defined in terms of the appropriate resistance values and the voltage reference, A_{ref}.

$$V_{out1} = V_{ref}\left[\left(\frac{R_{3L}}{R_3}\right) - \left(\frac{R_S}{VR_2}\right)\left(\frac{R_{3U}}{R_3}\right)\right] + V_a\left(\frac{R_{3U}}{R_3}\right)\left[\left(\frac{R_S}{R_2}\right) + 1\right]$$

$$V_{ref} = V_a\left(1 + \frac{R_1}{R_5}\right) - 5\left(\frac{R_1}{R_5}\right)$$

By adding the non-inverting amplifier, the final gain can be applied to the circuit and the voltage output of the linearized Wheatstone bridge, $V_{out1,}$ can be converted into the voltage output of the entire circuit, V_{out}.

The non-inverting amplifier portion of the circuit is repeated in Fig. 3.5.

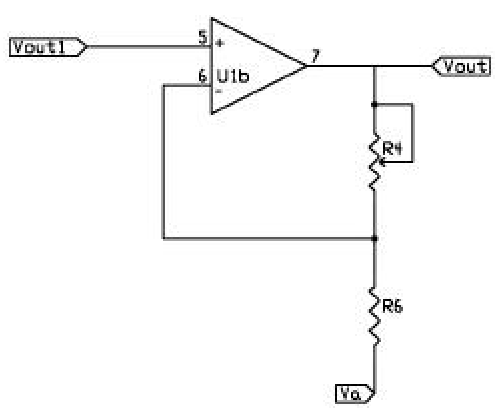

Figure 3.5 Non-inverting amplifier

From Figure 3.5, the voltage output of the entire circuit has been defined in terms of the voltage output of the linearized Wheatstone bridge, V_{out1}, the appropriate resistance values, and the voltage reference, A_{ref}.

$$V_{out} = \left(V_{out1} - V_a\right)\left(1 + \frac{R_4}{R_6}\right) + V_a$$

By substituting the equation for V_{out1}, the final equation for the output voltage of the entire circuit can be derived.

$$V_{out} = \left(V_{ref}\left[\left(\frac{R_{3L}}{R_3}\right) - \left(\frac{R_S}{R_2}\right)\left(\frac{R_{3U}}{R_3}\right)\right] + V_a\left(\frac{R_{3U}}{R_3}\right)\left[\left(\frac{R_S}{R_2}\right) + 1\right] - V_a\right)\left(1 + \frac{R_4}{R_6}\right) + V_a$$

After careful manipulation of the equation for V_{out}, three equations have been obtained that can be used to calculate the sensor resistance. All of the variables that are needed to calculate the sensor resistance are stored in the LabVIEW® program during execution. LabVIEW® then computes the following equations.

$$R_S = \left(\frac{R_2}{V_a - V_{ref}}\right)\left[V_{out1}\left(\frac{R_3}{R_{3U}}\right) - V_{ref}\left(\frac{R_{3L}}{R_{3U}}\right) - V_a\right]$$

$$V_{ref} = V_a\left(1 + \frac{R_1}{R_5}\right) - 5\left(\frac{R_1}{R_5}\right) \qquad V_{out1} = \frac{V_{out} \cdot R_6 - V_a \cdot R_4}{R_6 + R_4}$$

3.4.2 Variable Resistors

The four programmable variable resistors used were packaged in a 24 pin Dual Inline Package (DIP) from Analog Devices. This chip is also available in a surface mount package. Its' designation is the AD8403 and it comes in 1K, 10K, 50K, and 100K ohm sizes. All four potentiometers in the various packages have the same value. The resistor value that is used in this project is 1K ohm. The AD8403 can be programmed via a 3-wire serial program interface (SPI), see Figure 3.6.

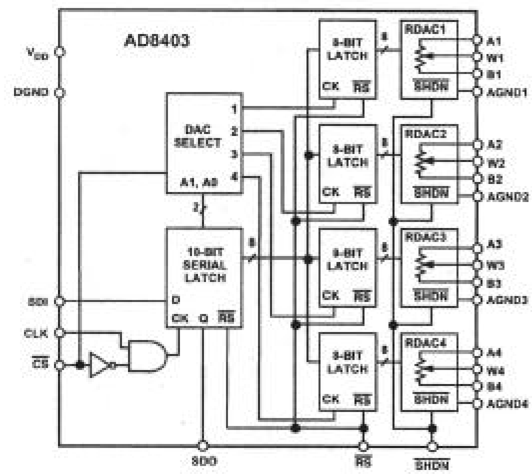

Figure 3.6 AD8403 block diagram [2]

As shown in Figure 3.7, the variable resistor inside the AD8403 is a series of small resistors and transmission gates. It has 256 positions. For the 1K ohm resistors used for this project, the smallest resistance available is

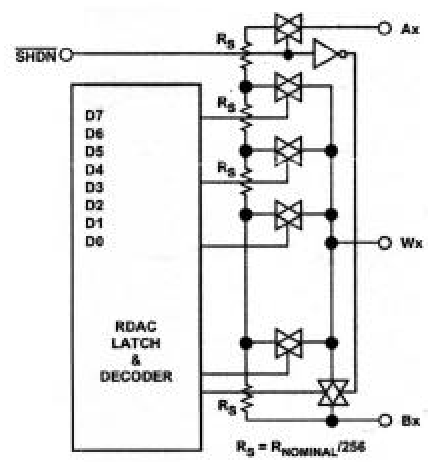

Figure 3.7 AD8403 circuit diagram [2]

$R = \dfrac{R_{NOMINAL}}{256} + R_{WIPER}$. Since the nominal resistance is 1200 ohms and the wiper resistance is 47 ohms [2], the smallest resistance available at the device outputs is approximately 52 ohms.

Resistance values are changed by clocking a 10-bit serial data word into the serial data input pin of the variable resistor. Of the 10-bit serial data word, 2-bits are address bits and 8-bits are data bits.

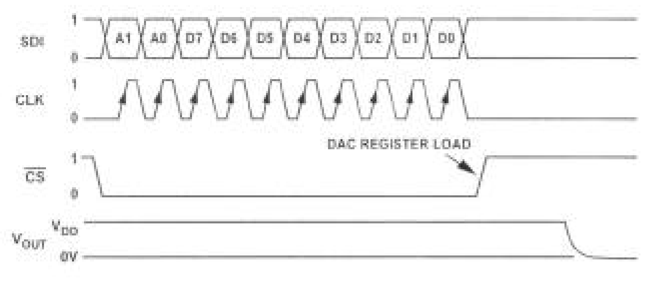

Figure 3.8 AD8403 timing diagram [2]

To program the resistor to a desired value, R_{WA}, a simple formula is used to calculate an appropriate data value, D_X. The equation for the data value is: $D_X = 256\left(1-\frac{R_{WA}-R_W}{R_{BA}}\right)$, where R_W is the wiper resistance, R_{BA} is the total resistance of the variable resistor, and R_{WA} is the desired resistance.

The 3-wire serial program interface consists of a serial data input, a clock input, and a chip select input. The timing diagram in Figure 3.8 shows the timing relationship between the three signals [2]. The chip select input is essentially a low enable that is required to activate the chip. Once the enable is toggled low, the clock and the data input can be activated. The data is clocked into a serial latch in the AD8403 on the positive transition of the clock signal. When the chip select signal toggles high, the data is clocked into the appropriate variable resistor determined from the two address bits.

3.4.3 Theoretical circuit error

In this chapter, a circuit is presented which aids in the calculation of sensor resistance R_S. How precise is the value we obtain? If we have a quantity, ‘R_S,’ that is a function of ‘n’ independent variables, then: $R_S = f(n_1, n_2, n_3, \cdots n_n)$ and each of the quantities has imprecision, $\pm \Delta n$.

The imprecision associated with the DAQ-1200 card is 0.12%.

The imprecision associated with the AD8403 variable resistors is 1.95%.

The imprecision of the function R_S can be written as:

$$\pm \Delta n = \sqrt{\left(\Delta n_1 \cdot \frac{\partial R_S}{\partial n_1}\right)^2 + \left(\Delta n_2 \cdot \frac{\partial R_S}{\partial n_2}\right)^2 + \left(\Delta n_3 \cdot \frac{\partial R_S}{\partial n_3}\right)^2 + \cdots + \left(\Delta n_n \cdot \frac{\partial R_S}{\partial n_n}\right)^2}$$

In this circuit, R_S has an imprecision of 12.6%. The equation for R_S and the equations for the partial derivatives are shown below and on the next page. The computation of the imprecision was performed using a MATLAB program. The variables of interest are V_{out}, R_1, R_2, R_3, R_{3U}, R_{3L}, and R_4.

$$R_S = \frac{V_{out} \cdot R_2 \cdot R_3 \cdot R_6 \cdot R_5}{R_1 \cdot R_{3U}(A_{ref}+5)(R_4+R_6)} - \frac{A_{ref} \cdot R_2 \cdot R_3 \cdot R_4 \cdot R_5}{R_1 \cdot R_{3U}(A_{ref}+5)(R_4+R_6)} - \frac{A_{ref} \cdot R_2 \cdot R_{3L}}{R_{3U}(A_{ref}+5)}$$

$$- \frac{A_{ref} \cdot R_2 \cdot R_{3L} \cdot R_5}{R_1 \cdot R_{3U}(A_{ref}+5)} + \frac{5 \cdot R_2 \cdot R_{3L}}{R_{3U}(A_{ref}+5)} - \frac{A_{ref} \cdot R_2 \cdot R_5}{R_1(A_{ref}+5)}$$

$$\frac{\partial R_S}{\partial V_{out}} = -\frac{R_2 \cdot R_3 \cdot R_6 \cdot R_5}{R_1 \cdot R_{3U}(A_{ref}+5)(R_4+R_6)}$$

$$\frac{\partial R_S}{\partial VR_1} = -\frac{V_{out} \cdot R_2 \cdot R_3 \cdot R_6 \cdot R_5}{R^2{}_1 \cdot R_{3U}(A_{ref}+5)(R_4+R_6)} + \frac{A_{ref} \cdot R_2 \cdot R_3 \cdot R_4 \cdot R_5}{R^2{}_1 \cdot R_{3U}(A_{ref}+5)(R_4+R_6)}$$

$$+ \frac{A_{ref} \cdot R_2 \cdot R_{3L} \cdot R_5}{R^2{}_1 \cdot R_{3U}(A_{ref}+5)} + \frac{A_{ref} \cdot R_2 \cdot R_5}{R^2{}_1(A_{ref}+5)}$$

$$\frac{\partial R_S}{\partial VR_2}=\frac{V_{out}\cdot R_3\cdot R_6\cdot R_5}{R_1\cdot R_{3U}\left(A_{ref}+5\right)\left(R_4+R_6\right)}-\frac{A_{ref}\cdot R_3\cdot R_4\cdot R_5}{R_1\cdot R_{3U}\left(A_{ref}+5\right)\left(R_4+R_6\right)}-\frac{A_{ref}\cdot R_{3L}}{R_{3U}\left(A_{ref}+5\right)}$$

$$-\frac{A_{ref}\cdot R_{3L}\cdot R_5}{R_1\cdot R_{3U}\left(A_{ref}+5\right)}+\frac{5\cdot R_{3L}}{R_{3U}\left(A_{ref}+5\right)}-\frac{A_{ref}\cdot R_5}{R_1\left(A_{ref}+5\right)}$$

$$\frac{\partial R_S}{\partial VR_3}=\frac{V_{out}\cdot R_2\cdot R_6\cdot R_5}{R_1\cdot R_{3U}\left(A_{ref}+5\right)\left(R_4+R_6\right)}-\frac{A_{ref}\cdot R_2\cdot R_4\cdot R_5}{R_1\cdot R_{3U}\left(A_{ref}+5\right)\left(R_4+R_6\right)}$$

$$\frac{\partial R_S}{\partial VR_{3U}}=-\frac{V_{out}\cdot R_2\cdot R_3\cdot R_6\cdot R_5}{R_1\cdot R^2{}_{3U}\left(A_{ref}+5\right)\left(R_4+R_6\right)}+\frac{A_{ref}\cdot R_2\cdot R_3\cdot R_4\cdot R_5}{R_1\cdot R^2{}_{3U}\left(A_{ref}+5\right)\left(R_4+R_6\right)}$$

$$+\frac{A_{ref}\cdot R_2\cdot R_{3L}}{R^2{}_{3U}\left(A_{ref}+5\right)}+\frac{A_{ref}\cdot R_2\cdot R_{3L}\cdot R_5}{R_1\cdot R^2{}_{3U}\left(A_{ref}+5\right)}-\frac{5\cdot R_2\cdot R_{3L}}{R^2{}_{3U}\left(A_{ref}+5\right)}$$

$$\frac{\partial R_S}{\partial VR_{3L}}=-\frac{A_{ref}\cdot R_2}{R_{3U}\left(A_{ref}+5\right)}-\frac{A_{ref}\cdot R_2\cdot R_5}{R_1\cdot R_{3U}\left(A_{ref}+5\right)}+\frac{5\cdot R_2}{R_{3U}\left(A_{ref}+5\right)}$$

$$\frac{\partial R_S}{\partial VR_4}=-\frac{V_{out}\cdot R_2\cdot R_3\cdot R_6\cdot R_5}{R_1\cdot R_{3U}\left(A_{ref}+5\right)\left(R_4+R_6\right)^2}+\frac{A_{ref}\cdot R_2\cdot R_3\cdot R_4\cdot R_5}{R_1\cdot R_{3U}\left(A_{ref}+5\right)\left(R_4+R_6\right)^2}$$

$$-\frac{A_{ref}\cdot R_2\cdot R_3\cdot R_5}{R_1\cdot R_{3U}\left(A_{ref}+5\right)\left(R_4+R_6\right)}$$

It is easy to see from the equations shown above the complexity in the computation of the imprecision of the circuit.

3.4.4 LabVIEW® control program

The LabVIEW® control program has several important functions: (1) it enables the control of the variable resistors using a 3-wire Serial Program Interface (SPI), (2) it computes the sensor resistance value, (3) it compensates for sensor drift.

- **3-Wire Serial Program Interface**

  The 3-wire SPI was developed using the DAQ-1200 card and LabVIEW® to facilitate the programming of the variable resistors. Initially it was considered trivial to enable a clock signal and then to synchronize the output data. Providing this feature turned out to be nontrivial. The problem was traced to the DAQ-1200 card which has three clock signals built into it. All three were necessary to generate a pulse train for the SPI. This did not leave any extra clock signals for other timing events such as synchronizing the data to the pulse train. Consequently, the pulse train was built manually along with the enable signal and the data output. All three signals were then combined electronically and output through an 8-line digital port. Correct timing was accomplished internally by incorporating a time delay in the LabVIEW® code; this timing was subsequently used to program the variable resistors.

- **Sensor Resistance Computation**

  Computing the actual sensor resistance accurately is a software function. Since the values of all the circuit components are stored in the LabVIEW® control program, computing the actual sensor value is just a matter of programming the equations in LabVIEW®. The LabVIEW® sensor resistance computation is shown in Figure 3.9.

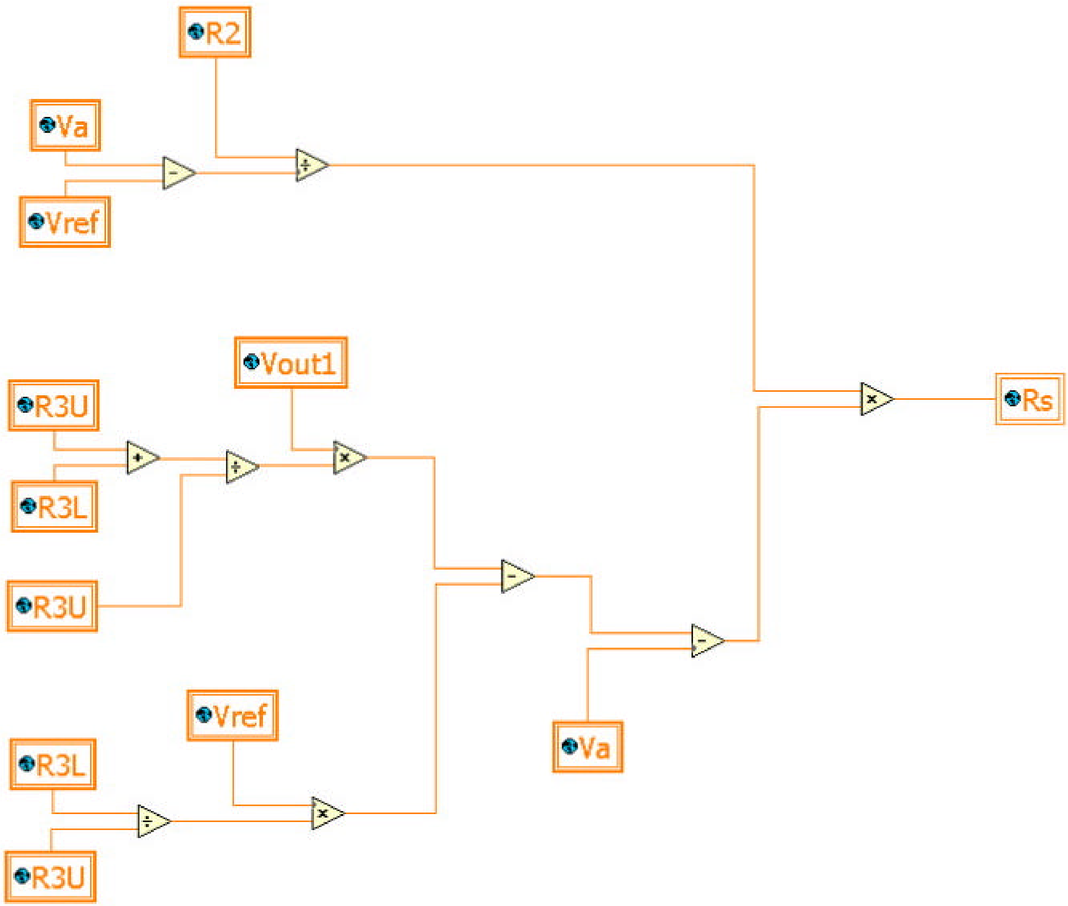

Figure 3.9 LabVIEW® sensor resistance computation

As can be seen in Figure 3.9, all the values for the variable resistor are stored as global variables. The variables designated V_{ref} and V_{out1} are computed earlier in the program. By using global variables, these values can be passed in and out of the sequence structures efficiently and effectively when required.

- **Search Algorithm**

  A search algorithm is included in the control program to find the optimal value of resistance that will balance the Wheatstone bridge. The search algorithm starts by setting the resistance value of R2 to its minimum. The value of R2 is incremented and the voltage output of the circuit is monitored. This forward search executes continuously until the output voltage of the circuit is minimized to the analog reference voltage. The search algorithm initially steps past the 'ideal' resistance value and then reverses direction in a local search to determine the optimum resistance value to be used. One disadvantage to this type of search is that it can get stuck in a local minimum.

- **LabVIEW® program structure**

The structure of the LabVIEW® control program involves circuit initialization, monitoring of the sensor resistance, and sensor drift compensation. A block diagram of the structure is shown in Figure 3.10.

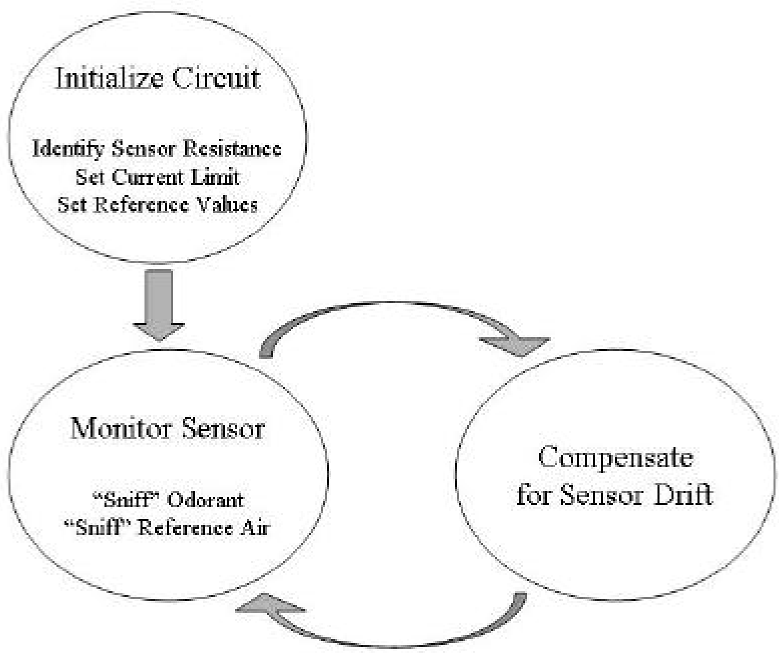

Figure 3.10 LabVIEW® Program Structure

As shown in Figure 3.10, the function of the circuit initialization is to set the current limit and set initial reference values for each variable resistor. The sensor resistance will be monitored and sampled during the duration of the "sniff." After each "sniff" and reference cycle, the LabVIEW® control program adjusts the balance of the bridge to achieve a minimum voltage output with respect to the analog reference. This approach compensates for the sensor drift. The program then continues on to the next odorant connected to the auto-sampler. The sensor sampling and drift compensation continues in a loop until all the odorants have been sampled the designated number of times.

3.5 Experimental results

In an electronic nose application, up to 32 channels of adaptive electronic circuits might be necessary. To prove the concept of adaptive electronics, only one channel was tested in this project. There are always improvements that can be made. Once the appropriate changes have been determined in the design, a multi-channel adaptive electronic interface may be implemented. Figure 3.11 is a photograph of the experiment testing the single channel implementation of an adaptive electronic interface.

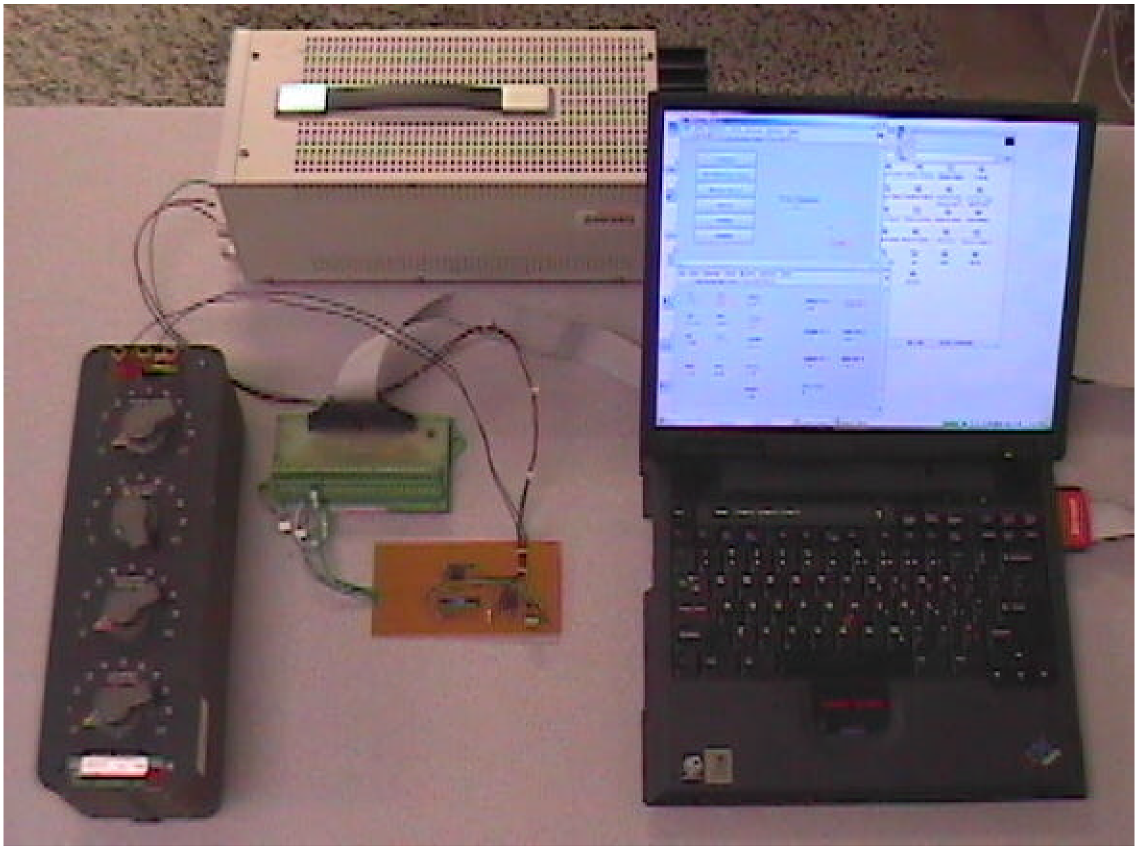

3.11 Experimental setup

3.5.1 Experimental Setup

A single channel of the adaptive electronics has been built and tested (see Figure 3.11). A schematic capture of the printed circuit board layout is shown in Figure 3.12. The board was milled in the Electrical and Computer Engineering Department using a single-sided copper circuit board.

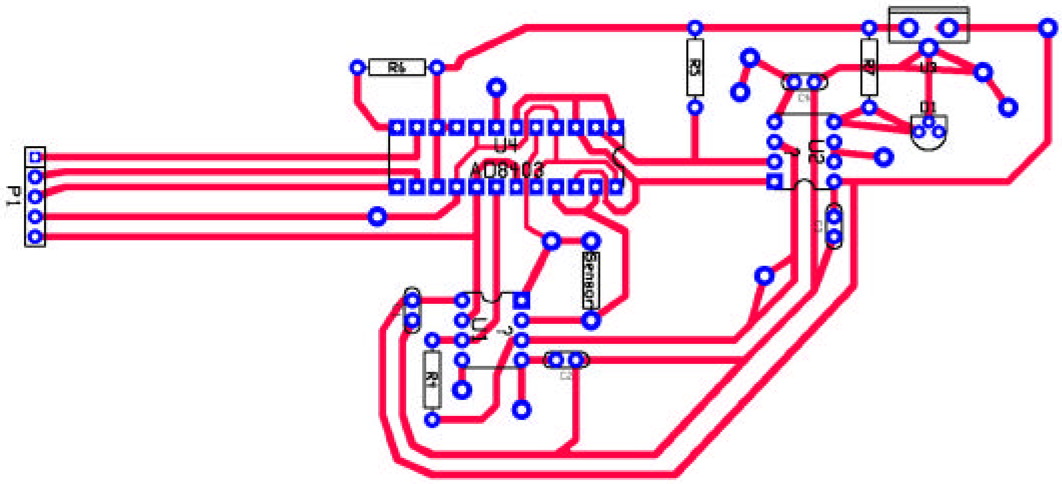

Figure 3.12 Printed Circuit Board

A photograph of the adaptive electronics circuit is shown in Figure 3.13. The circuit was rapidly prototyped using a single sided PCB and a milling machine in the Center for Robotics and Intelligent Machines.

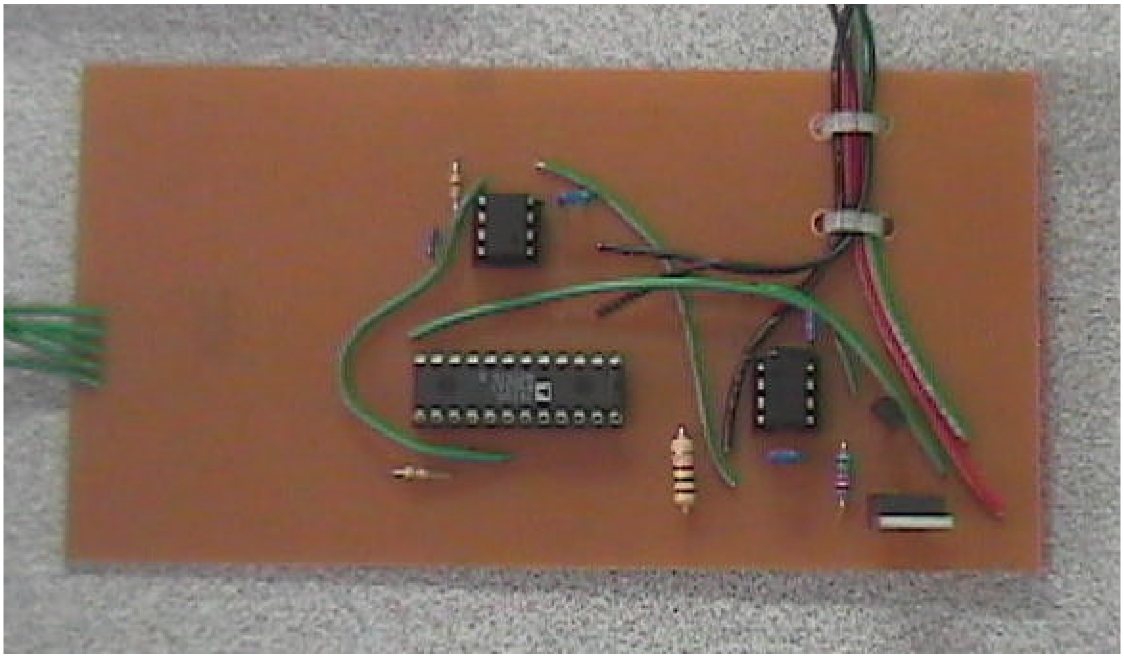

Figure 3.13 Photo of adaptive electronics circuit

3.5.2 Circuit Performance

Table 5 shows the actual circuit error for different ranges of resistance values. The average error for the entire range of the circuit is 8% with a maximum error of 11.16%. The error in the circuit is due to the imprecision in the DAQ-1200 card and the AD8403 variable resistors. A calibration algorithm has been written and implemented to compensate for the error in each 100 ohm range. Table 6 shows the actual circuit error after a calibration has been performed. After calibration, the average error for the entire range of the circuit is 0.18% with a maximum error of 0.81%.

Due to the variations that can occur in the AD8403 and the DAQ-1200 card, when the circuit power is cycled on and off, the circuit error may change. Because of this, a calibration must be performed each time the circuit is powered up.

Table 5. Pre-Calibration Data

Decade Resistor Box Setting	Actual Resistance Value	LabVIEW® Computed Resistance Value	Difference Between Measured Value and LabVIEW® Computed Value (ohms)	Difference Between Measured Value and LabVIEW® Computed Value (%)	Average Error (%)
100	99.99	108.3	8.31	8.31	
110	109.98	118.4	8.42	7.66	
120	119.97	128.5	8.53	7.11	
130	129.97	138.8	8.83	6.79	
140	139.96	149.4	9.44	6.74	
150	149.96	160.2	10.24	6.83	
160	159.96	170.7	10.74	6.71	
					7.17
200	199.9	222.2	22.3	11.16	
210	209.8	232.8	23	10.96	
220	219.7	243.4	23.7	10.79	
230	229.7	254.2	24.5	10.67	
240	239.7	265.4	25.7	10.72	
250	249.7	276.6	26.9	10.77	
260	259.7	287.5	27.8	10.70	
					10.82
300	299.7	321.9	22.2	7.41	
310	309.7	332	22.3	7.20	
320	319.6	342.1	22.5	7.04	
330	329.6	352.4	22.8	6.92	
340	339.6	362.9	23.3	6.86	
350	349.6	373.8	24.2	6.92	
360	359.5	384.4	24.9	6.93	
					7.04
400	399.5	433.1	33.6	8.41	
410	409.5	443.1	33.6	8.21	
420	419.5	453.4	33.9	8.08	
430	429.5	463.6	34.1	7.94	
440	439.5	474.3	34.8	7.92	
450	449.4	485.1	35.7	7.94	
460	459.4	495.9	36.5	7.95	
					8.06
500	499.9	536.3	36.4	7.28	
510	509.9	546.2	36.3	7.12	
520	519.9	556.3	36.4	7.00	
530	529.9	566.5	36.6	6.91	
540	539.9	576.9	37	6.85	
550	549.9	587.6	37.7	6.86	
560	559.9	598.1	38.2	6.82	
					6.98

Table 6. Post-Calibration Data

Decade Resistor Box Setting	Actual Resistance Value	LabVIEW® Computed Resistance Value	Difference Between Measured Value and LabVIEW® Computed Value (ohms)	Difference Between Measured Value and LabVIEW® Computed Value (%)	Average Error (%)
100	99.99	100.8	0.81	0.81	
110	109.98	110.5	0.52	0.47	
120	119.97	119.9	0.07	0.06	
130	129.97	129.6	0.37	0.28	
140	139.96	139.5	0.46	0.33	
150	149.96	149.5	0.46	0.31	
160	159.96	159.2	0.76	0.48	
					0.39
200	199.9	200.6	0.7	0.35	
210	209.8	210.1	0.3	0.14	
220	219.7	219.7	0	0.00	
230	229.7	229.5	0.2	0.09	
240	239.7	239.6	0.1	0.04	
250	249.7	249.8	0.1	0.04	
260	259.7	259.6	0.1	0.04	
					0.10
300	299.7	300.7	1	0.33	
310	309.7	310	0.3	0.10	
320	319.6	319.6	0	0.00	
330	329.6	329.3	0.3	0.09	
340	339.6	339	0.6	0.18	
350	349.6	349.3	0.3	0.09	
360	359.5	359.1	0.4	0.11	
					0.13
400	399.5	400.6	1.1	0.28	
410	409.5	410.2	0.7	0.17	
420	419.5	419.7	0.2	0.05	
430	429.5	429.2	0.3	0.07	
440	439.5	439	0.5	0.11	
450	449.4	449.1	0.3	0.07	
460	459.4	458.9	0.5	0.11	
					0.12
500	499.9	501	1.1	0.22	
510	509.9	510.3	0.4	0.08	
520	519.9	519.7	0.2	0.04	
530	529.9	529.2	0.7	0.13	
540	539.9	538.9	1	0.19	
550	549.9	549	0.9	0.16	
560	559.9	558.9	1	0.18	
					0.14

3.6 Conclusions

A single channel of an adaptive electronic interface for gas sensors has been designed, built, and tested. Its performance has been shown to be an improvement over the existing circuits used in the NC State E-Nose. The adaptive interface can be calibrated to an accuracy of at least 99%. The adaptive interface also allows for a direct mapping from the circuit output voltage to the sensor resistance. This allows for a more accurate analysis of sensor characteristics. Multiple channels of the adaptive interface can be implemented to accommodate any number of sensors.

3.7 References

[1] Shetty, D. and Kolk, R.A. Mechatronics System Design. Boston: PWS Publishing Company, 1997.

[2] Analog Devices "AD8403 Data Sheet." Revision B http://www.analog.com/productSelection/pdf/1867_b.pdf (date)

Chapter 4. Conclusions and Future Work

The electronic nose is aimed at replicating the functionality of the human nose. As the potential applications are numerous and sensors are designed to respond to a wide range of odors, sensor response must be accurately measured. Analog interface circuitry that is accurate and adaptable to many types of sensors must be developed. The work reported herein is an important step in achieving this goal. In this chapter we have summarized the work that we have done this far, our conclusions and future work we suggest.

4.1 Summary

Two main objectives were accomplished in this thesis. Both an adaptive electronic interface and a new conducting polymer sensor chamber were designed and tested.

The new conducting polymer sensor chamber was designed to address several problems with the existing chamber. Both the excessive volume and the unequal timing of the odorant to the sensors were corrected. In the process of attempting to address the issue of turbulence using a new “sniff and hold” mode, it was discovered that the conducting polymer sensors that were being used were reacting to the change in flow rate as well as the odorant in the chamber.

The adaptive electronic interface was designed to address several problems that existed with the original interface circuit. Two problems that the original circuit had were that there was not an accurate way to determine the sensor resistance from the circuit voltage output and the Wheatstone bridge in the original circuit was nonlinear. The potentiometers in the original circuit were adjusted for a visual response only. The existing design does not allow the actual values of the potentiometers or the gain of the circuit to be recorded. Because of this, mapping the circuit voltage output back to the actual sensor resistance was not feasible. These problems were resolved using a linearized Wheatstone bridge in the new circuit and using programmable variable resistors to make all adjustments via a LabVIEW® control program. Using the programmable variable resistors and the LabVIEW® control program also allows for compensation of sensor drift.

4.2 Future Work

A single channel of the adaptive electronic interface was built and tested. A larger multi-channel adaptive electronic interface should be designed and implemented in the NC State E-Nose. This will make the NC State E-Nose a more flexible research tool.

More research should also be done on the effect of gas flow rate on sensor response. Whether or not an ideal flow rate exists for different types of sensors is an important question for future study.

Appendix

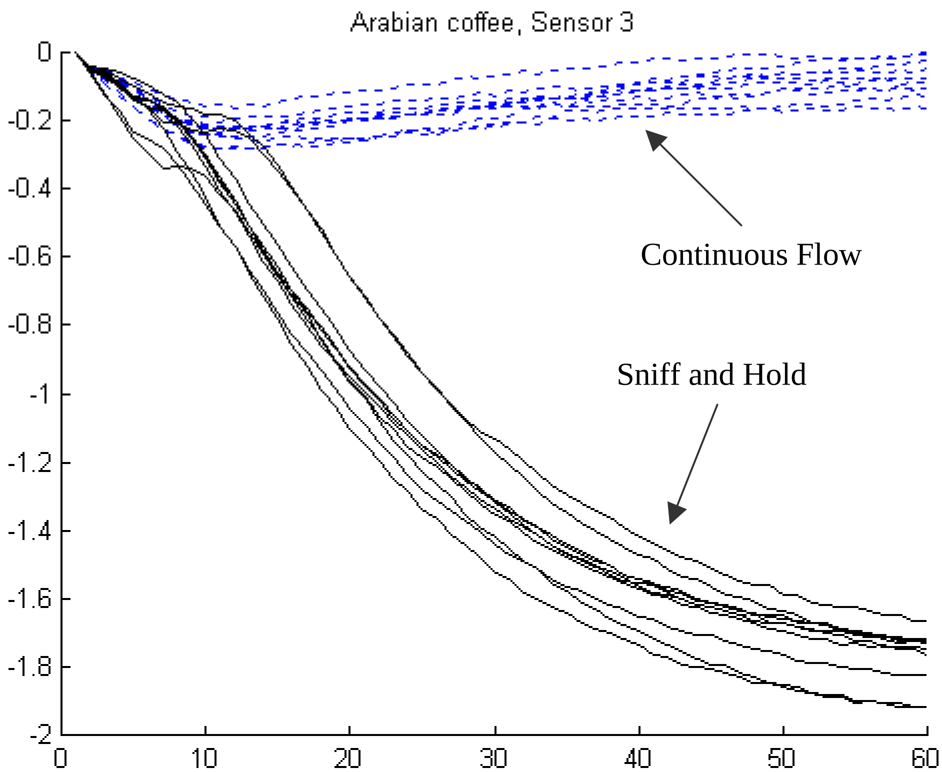

Figure A.1 Arabian Coffee, Sensor 3

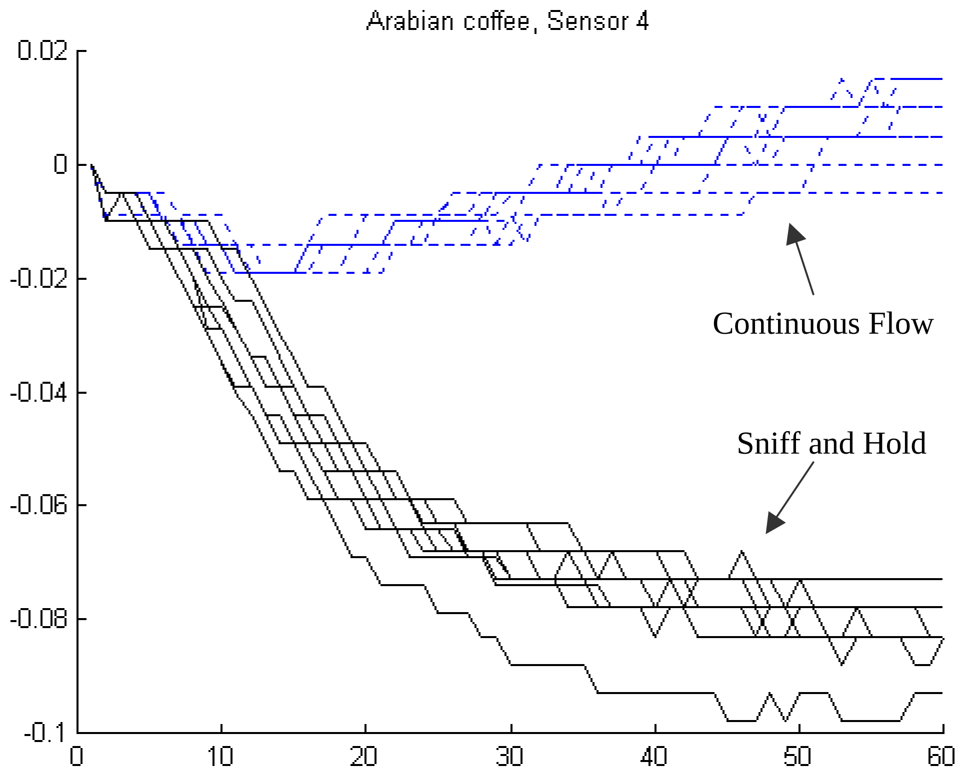

Figure A.2 Arabian Coffee, Sensor 4

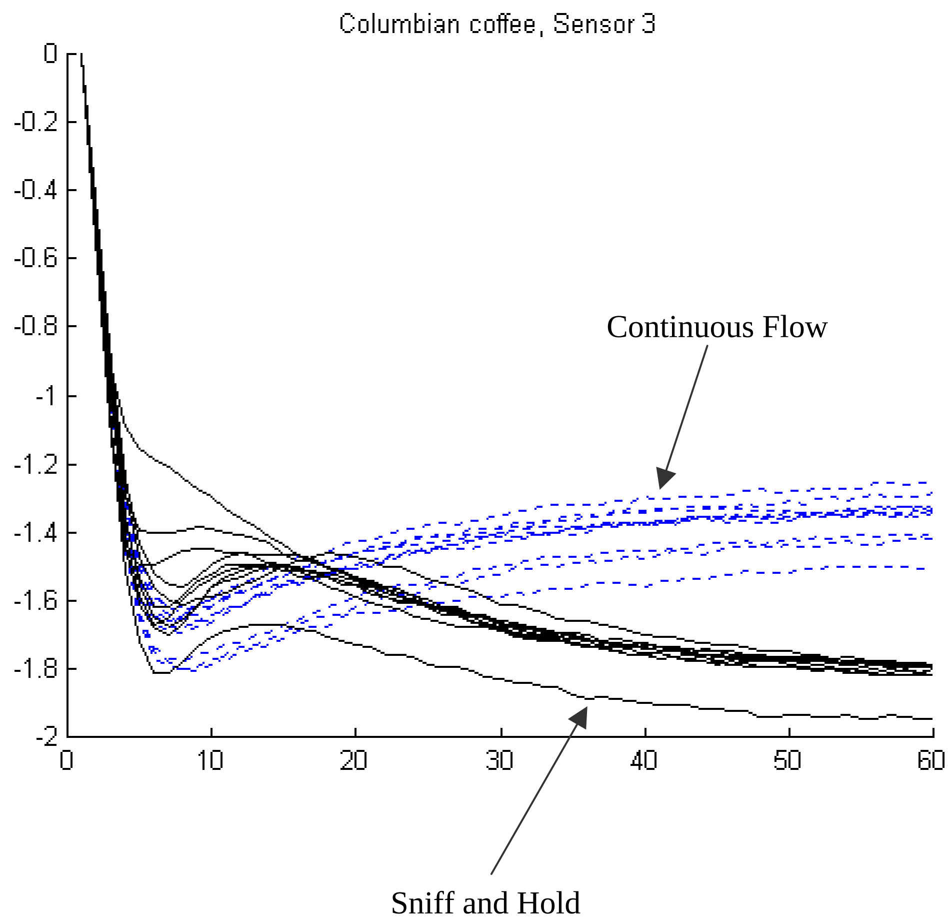

Figure A.3 Columbian Coffee, Sensor 3

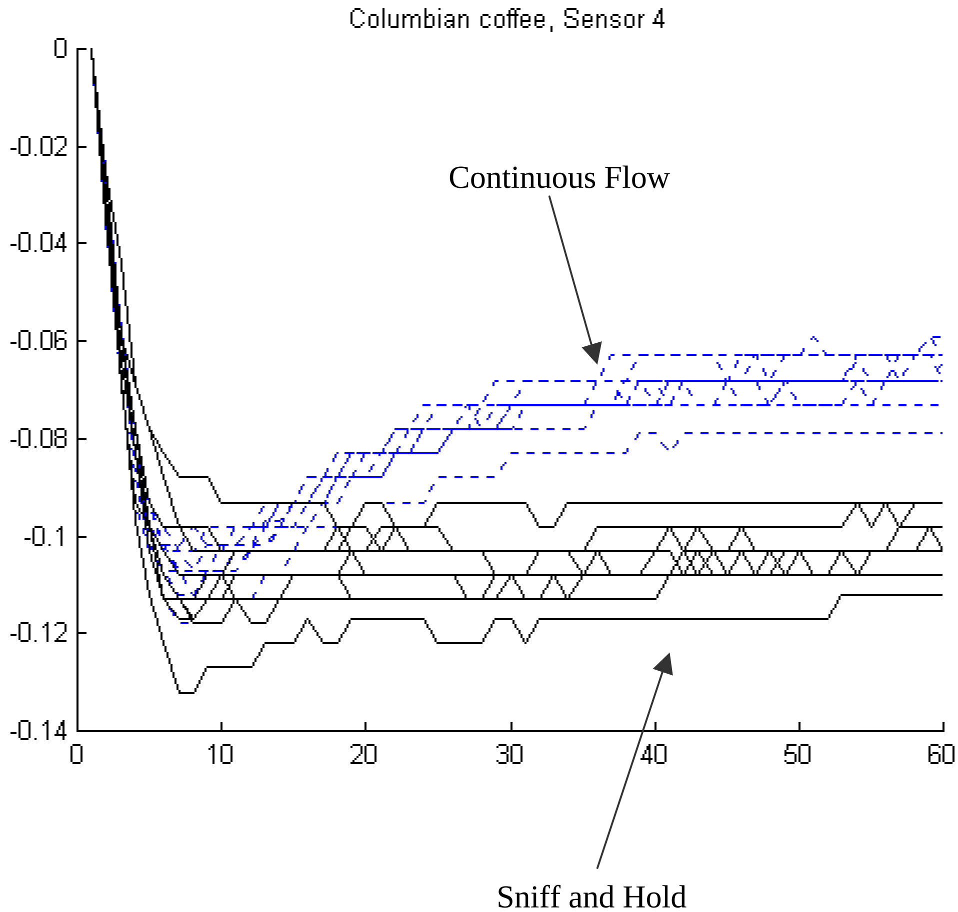

Figure A.4 Columbian Coffee, Sensor 4

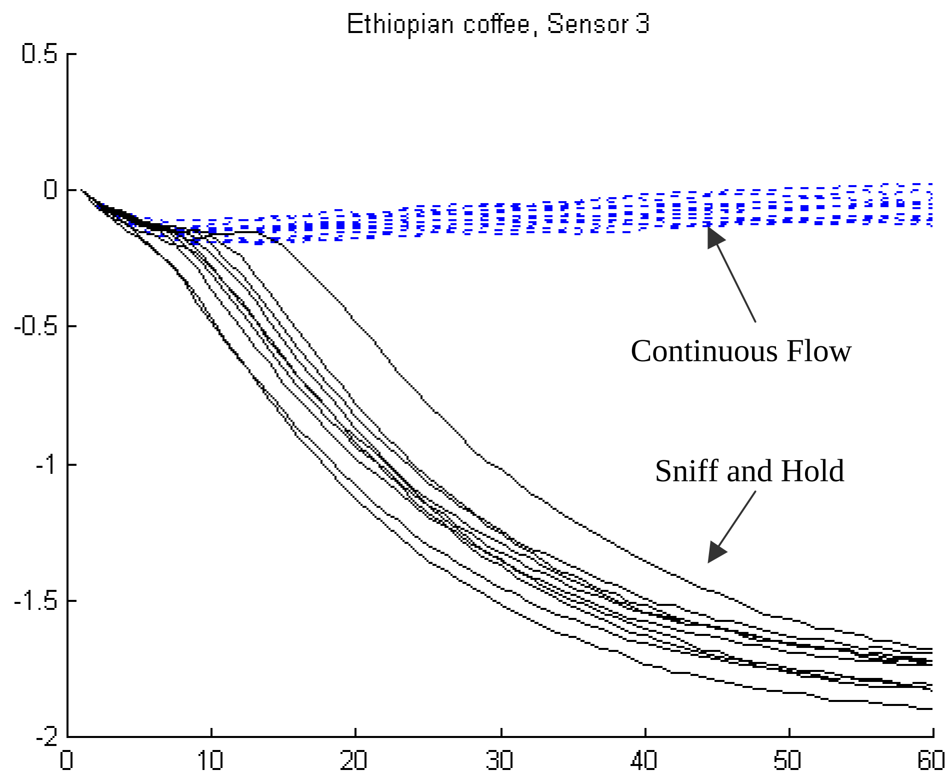

Figure A.5 Ethiopian Coffee, Sensor 3

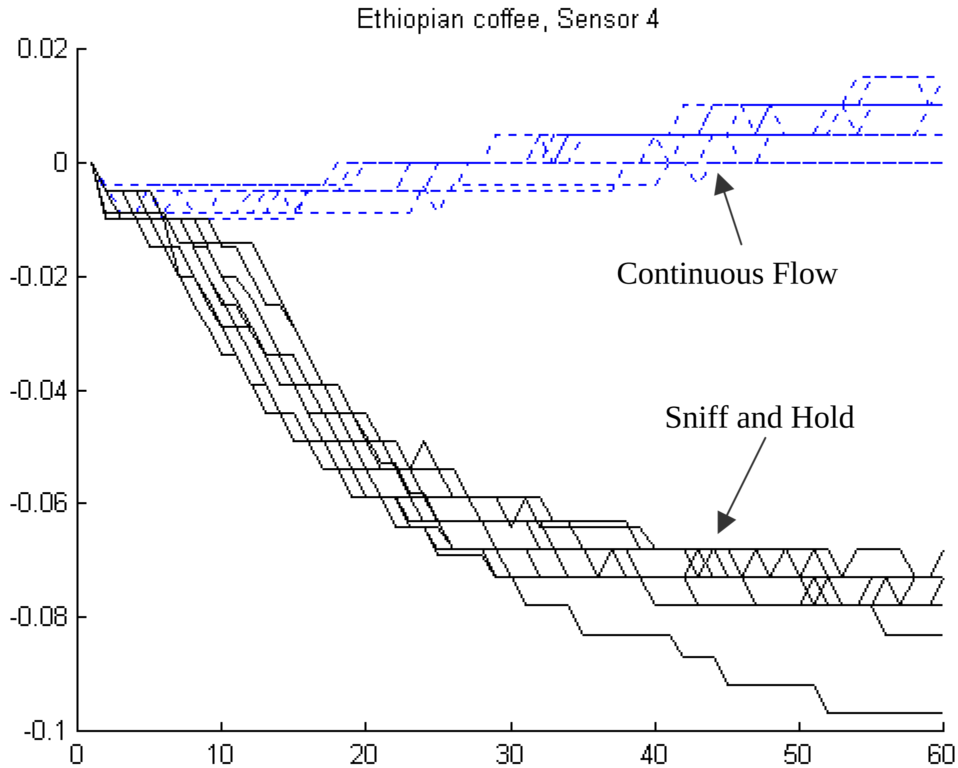

Figure A.6 Ethiopian Coffee, Sensor 4

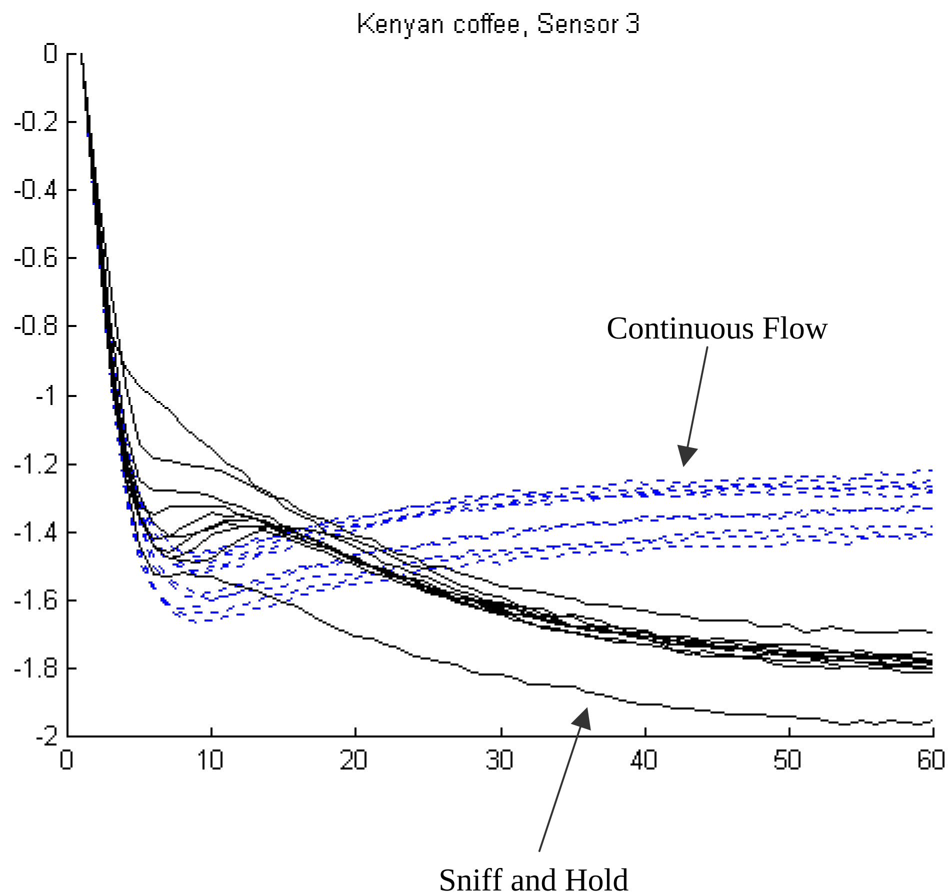

Figure A.7 Kenyan Coffee, Sensor 3

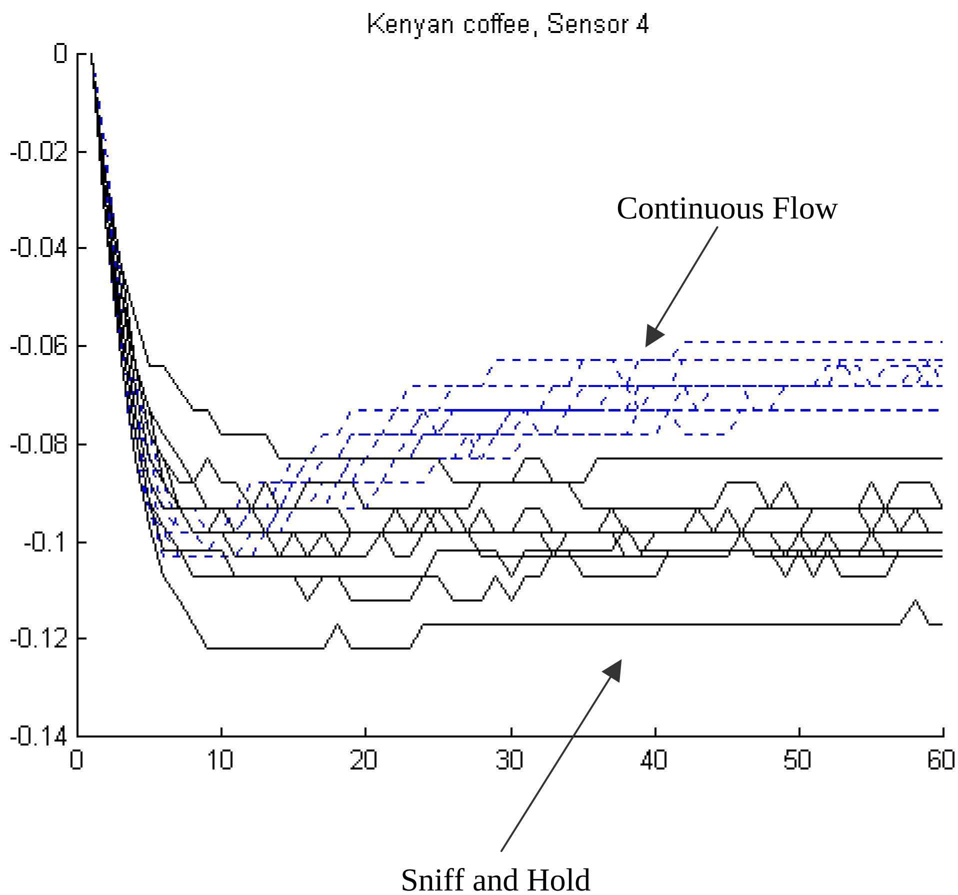

Figure A.8 Kenyan Coffee, Sensor 4